

A MATHEMATICAL STUDY OF THE EFFECT  
OF A MOVING BOUNDARY AND A  
THERMAL BOUNDARY LAYER ON  
DROPLET HEATING AND EVAPORATION

IVAN GUSEV

PHD

2012

A MATHEMATICAL STUDY OF THE EFFECT  
OF A MOVING BOUNDARY AND A  
THERMAL BOUNDARY LAYER ON  
DROPLET HEATING AND EVAPORATION

IVAN GUSEV

A thesis submitted in partial fulfillment of the  
requirements of the University of Brighton  
for the degree of Doctor of Philosophy

January 2012

Sir Harry Ricardo Laboratories  
The University of Brighton

## Abstract

Two new solutions to the heat conduction equation, describing transient heating of an evaporating droplet, are suggested. Both solutions take into account the effect of the reduction of the droplet radius due to evaporation, assuming that this radius is a linear function of time. It has been pointed out that the new approach predicts lower droplet surface temperatures and slower evaporation rates compared with the traditional approach. New solutions to the heat conduction equation, describing transient heating of an evaporating droplet, are suggested, assuming that the time evolution of droplet radius  $R_d(t)$  is known. The results of calculations are compared with the results obtained using the previously suggested approach, when the droplet radius was assumed to be a linear function of time during individual time steps, for typical Diesel engine-like conditions. Both solutions predict the same results which indicates that both models are likely to be correct.

Two new solutions to the equation, describing the diffusion of species during multi-component droplet evaporation, are suggested. The first solution is the explicit analytical solution to this equation while the second one reduces the solution of the differential species diffusion equation to the solution of the Volterra integral equation of the second kind. Both solutions take into account the effect of the reduction of the droplet radius due to evaporation, assuming that this radius is a linear function of time. The analytical solution has been incorporated into a zero dimensional CFD code and applied to the analysis of bi-component (50% ethanol { 50% acetone mixture) droplet evaporation at atmospheric pressure.

The transient heat conduction equation, describing heating of a body immersed into gas with inhomogeneous temperature distribution, is solved analytically, assuming that, at a certain distance from the body, gas temperature remains constant. The solution is applied to modelling of body heating in conditions close to those observed in Diesel engines. In the long time limit, the distribution of temperature in the body and gas practically does not depend on the initial distribution of gas temperature.

# Contents

Abstract	i
Contents	ii
List of Tables	iii
List of Figures	iv
Acknowledgements	ix
Declaration	x
Nomenclature	xi
<b>1 Introduction</b>	<b>1</b>
1.1 Motivation . . . . .	1
1.2 Background research . . . . .	2
1.3 Structure of the thesis . . . . .	6
<b>2 Transient heating of an evaporating droplet when droplet is a linear function of time</b>	<b>8</b>
2.1 Introc(In)28e . . . . .	2
1sicMotskgrouapp00128turm1(Mots)285 . . . . .	

2.5	Numerical vs analytical solutions . . . . .	30
2.6	Conclusions of Chapter 2 . . . . .	33
<b>3</b>	<b>Transient heating of an evaporating droplet with presumed time evolution of its radius</b>	<b>35</b>
3.1	Introduction of Chapter 3 . . . . .	35
3.2	Solution for the case of arbitrary $R_d(t)$ but $T_{\infty}(R) = \text{const}$ . . . . .	36
3.3	Solution for the case of arbitrary $R_d(t)$ and $T_{\infty}(R)$ . . . . .	38
3.4	Implementation of the new solutions into a numerical code . . . . .	41
3.5	Results . . . . .	41
3.6	Conclusions of Chapter 3 . . . . .	52
<b>4</b>	<b>New solutions to the species diffusion equation inside droplets in the presence of the moving boundary</b>	<b>54</b>
4.1	Introduction of Chapter 4 . . . . .	54
4.2	Basic equations for multi-component droplets . . . . .	55
4.3	Analytical solution of Equation (4.1) . . . . .	58
4.4	Application to bi-component droplets . . . . .	66
4.4.1	Effect of species diffusion . . . . .	66
4.4.2	Combined effects of species and thermal diffusion . . . . .	70
4.5	Conclusions of Chapter 4 . . . . .	75
<b>5</b>	<b>Transient heating of a semitransparent spherical body immersed into a gas with inhomogeneous temperature distribution</b>	<b>78</b>
5.1	Introduction of Chapter 5 . . . . .	78
5.2	Basic equations and assumptions . . . . .	79
5.3	The analytical solution . . . . .	81
5.4	Analysis . . . . .	82
5.5	Conclusions of Chapter 5 . . . . .	87
<b>6</b>	<b>Conclusions</b>	<b>89</b>
	<b>References</b>	<b>93</b>
	<b>Appendices</b>	<b>107</b>

# List of Tables

4.1	Approximations of acetone, ethanol and their mixtures' droplet velocities. . . . .	70
4.2	The measured initial values of droplet temperature, diameter, ambient gas temperature and distance parameter for the same cases as in Table 4.1. . . . .	71

# List of Figures

2.1	A schematic presentation of the plot $R_d$ versus $t$ for an evaporating droplet (solid); approximation of this plot using the conventional approach assuming that $R_d = \text{const}$ during the time step (dotted); approximation of this plot using the new approach assuming that $R_d$ is the linear function of $t$ during each time step (dashed). . . . .	9
2.2	The plots of $\rho$ versus droplet surface temperature $T_s$ for $M_a = 29$ kg/kmole, $M_f = 170$ kg/kmole ( $C_{12}H_{26}$ ), $p = 3000$ kPa, $a = 15.5274$ , $b = 5383.59$ , $T_g = 1000$ K, and droplet initial radii $5 \mu\text{m}$ (a) and $50 \mu\text{m}$ (b). . . . .	23
2.3	The plots of $T$ versus $r = R - R_d$ for the same values of parameters as in Fig. 2.2 and various times (indicated near the curves). The calculations were performed using the new model, taking into account the evaporation process (solid), and ignoring the effects of evaporation (dotted) for $R_{d0} = 5 \mu\text{m}$ (a) and $R_{d0} = 50 \mu\text{m}$ (b). . . . .	25
2.4	The plots of $T_s$ versus time (a) and $R_d$ versus time (b) for heated and evaporating droplets using the conventional (dotted), and new (solid) approaches for $T_g = 1000$ K and $R_{d0} = 5 \mu\text{m}$ . . . . .	26
2.5	The same as Fig. 2.4 but for $R_{d0} = 10 \mu\text{m}$ . . . . .	27
2.6	The same as Fig. 2.4 but for $R_{d0} = 50 \mu\text{m}$ . . . . .	28
2.7	The values of $\frac{t_e(\text{new})}{t_e(\text{conventional})} = t_{e(\text{new})}$ versus $T_g$ for $T_g = 1000$ K and $R_{d0} = 5 \mu\text{m}$ . . . . .	29
2.8	The values of $\text{Error} = \frac{t_e(\text{time step}) - t_e(\text{time step}=0.003 \text{ ms})}{t_e(\text{time step}=0.003 \text{ ms})}$ versus time step for the conventional and new approaches for $T_g = 1000$ K and $R_{d0} = 5 \mu\text{m}$ . . . . .	30

2.9	Comparison of $T_s$ vs. $t$ obtained using three different methods: the box scheme (solid); the method developed in this chapter (dotted); and the conventional method for which $R(t)$ is piecewise constant in time (dashed). . . . .	31
2.10	Comparison of $R$ vs. $t$ obtained using three different methods: the box scheme (solid); the method developed in this chapter (dotted); and the conventional method for which $R(t)$ is piecewise constant in time (dashed). . . . .	32
3.1	The plots of $T_s$ versus time (a) and $R_d$ versus time (b) using the	



3.8	The same as Fig. 3.7 but for the general solution (Equation (3.23) applied to the case when the initial distribution of temperature inside the droplet is given by Equation (3.24)). . . . .	51
4.1	The plots of ethanol mass fraction $Y_{\text{eth}}$ versus $r = R=R_d$ , as predicted by the conventional model (dashed) and the new model, taking into account the effect of the moving boundary (solid), for times 0.001 s, 0.01 s and 0.03 s. We consider an initial 50% ethanol { 50% acetone mixture and droplets with initial diameter equal to 142.7 $\mu\text{m}$ . . . . .	67
4.2	The plots of $Y_{\text{eth}}(r = 1)$ versus time, as predicted by the conventional model (dashed) and the new model, taking into account the effect of the moving boundary (solid). . . . .	68
4.3	The plots of droplet radius $R_d$ versus time, as predicted by the conventional model (dashed) and the new model, taking into account the effect of the moving boundary (solid). . . . .	68
4.4	The plots of Spalding mass transfer number $B_M$ versus time, as predicted by the conventional model (dashed) and the new model, taking into account the effect of the moving boundary (solid). . . . .	69
4.5	The time evolution of droplet surface, average and centre temperatures ( $T_s$ , $T_{\text{av}}$ and $T_c$ ), predicted by the one-way Solution A for the non-ideal model, taking and not taking into account the effects of the moving boundary during individual time steps (moving and stationary boundaries) on the solutions to both heat transfer and species diffusion equations for the 25% ethanol { 75% acetone mixture droplets with the values of the initial parameters, droplet velocity and gas temperature given in Tables 4.1 and 4.2 (a); the same as (a) but for the 50% ethanol { 50% acetone mixture droplets (b). . . . .	72

4.6 The time evolution of droplet surface temperatures  $T_s(t)$  and radius  $(R_d)$ , predicted by the one-way Solution A for the non-ideal model, taking and not taking into account the effects of the moving boundary

# Acknowledgements

First of all I would like to thank my supervisors Prof. Sergei Sazhin and Prof. Morgan Heikal for their support during my work on this project. Also I am grateful to Dr. Pavel Krutitskii, Dr. Michael Vynnycky, Dr. Sarah Mitchell, Dr. Elena Sazhina, Dr. Guillaume Castanet, Prof. Fabrice Lemoine and Mr. Ahmed Elwardany for their criticism, support and valuable contributions to this work.

Last, but not least, I would like to thank my family and friends who gave me much inspiration and a moral boost.

Finally I am grateful to the European Regional Development Fund Franco-British INTERREG IVA (Project C5, Reference 4005) for the financial support of this project.

# Declaration

# Nomenclature

$a; b$	coefficients introduced in Equation (2.7) or $1 = \rho -$
$a_{b;g}$	coefficients introduced in Eq. (5.9) ( $\rho \bar{s}/m$ )
$b$	weight (see Appendix 7) [ $J/(m^3 K)$ ]
$A$	function defined by Eq. (A711)
$B$	function defined by Eq. (A711)
$B_M$	Spalding mass transfer number

$p$  pressure [Pa] or parameter introduced in Equation (4.23)  
 $p$

$W$	function introduced by Equation (2.17) or (4.14)
$X$	molar fraction
$Y$	mass fraction

### Greek symbols

	evaporation rate introduced in Equation (2.8)
$m$	parameter defined by Equation (4.3)
$\tau_0$	thermal 'lm' thickness [m]
	$(t_{e(new)} - t_{e(conventional)}) = t_{e(new)}$
$t$	time step [s]
$T$	$T_g - T_s$ [K]
	activity coefficient
	evaporation rate
	function defined by Equation (2.25) or (A61) or (4.22)
$s$	$\frac{T_s - T_0}{T}$
	function defined by Equation (4.44)
	thermal diffusivity (m <sup>2</sup> /s)
$\lambda_n$	eigenvalues defined by Equations (2.28), (4.26), (4.28) or (5.11)
$\theta(t)$	variable introduced by Equation (2.13) or (4.18)
$\hat{\theta}_0(t)$	variable introduced in Equation (4.49)
$\nu(t)$	function defined by Equation (3.5) or kinematic viscosity
$\omega(t; \cdot)$	function defined in Appendix 3
$\gamma(t; \cdot)$	function defined in Appendix 3
	$R = R_d(t)$
	parameter defined by Eq. (5.19)
$\rho$	parameter defined by Equation (4.6)
	density [kg/ m <sup>3</sup> ]
$\omega(t; 1)$	$W(t; 1)$

### Subscripts

$a$	air
amb	ambient

<i>b</i>	body or boiling
<i>d</i>	droplet
<i>e</i>	evaporation
<i>eff</i>	effective
<i>eth</i>	ethanol
<i>f</i>	fuel
<i>g</i>	gas
<i>i</i>	species
<i>iso</i>	isolated
<i>l</i>	liquid
<i>n</i>	timesteps in the integration
<i>p</i>	constant pressure
<i>part</i>	particular
<i>s</i>	surface
<i>v</i>	vapour
<i>0</i>	initial
<i>1</i>	ambient conditions



# Chapter 1

## Introduction

### 1.1 Motivation

heat conduction equation inside droplets. It was shown that this approach is more efficient, compared with the one based on the numerical solution to this equation, both from the point of view of accuracy and of CPU efficiency [16].

- 1) models based on the assumption that the droplet surface temperature is uniform and does not change with time;
- 2) models based on the assumption that there is no temperature gradient inside droplets (infinite thermal conductivity of liquid);
- 3) models taking into account finite liquid thermal conductivity, but not the re-circulation inside droplets (conduction limit);
- 4) models taking into account both finite liquid thermal conductivity and the re-circulation inside droplets via the introduction of a correction factor to the liquid thermal conductivity (effective conductivity models);
- 5) models describing the re-circulation inside droplets in terms of vortex dynamics (vortex models);

alternative approach was suggested and developed in [1, 15, 17, 52]. In these papers both finite liquid thermal conductivity and recirculation inside droplets (via the effective thermal conductivity (ETC) model [44]) were taken into account by incorporating the analytical solution to the heat conduction equation inside the droplet into a numerical scheme. The liquid thermal conductivity inside droplets was replaced by the effective thermal conductivity to take into account liquid recirculation

assumption that species inside droplets mix instantly quickly. Models containing features of both these groups of models have been suggested in [66]. Most of the models belonging to the first group are based on the numerical solution to the species diffusion equation inside droplets. At the same time the analysis of [38, 50] was based on the analytical solution to this equation. The model in [38] was applied to the analysis of heating and evaporation of bi-component ethanol/acetone droplets. The authors of [38] based their analysis on the analytical solution to the species diffusion equation, which was incorporated into the numerical code. This approach is expected to be more CPU efficient and accurate compared with the one based on the conventional approach [50]. The model described in [38] has been generalised in [50] to take into account coupling between droplets and gas. None of these models took into account the effects of the moving boundary due to evaporation on the species diffusion equation.

Most of the models of droplet heating and evaporation suggested so far are based on the assumption that gas in computational cells is always homogeneous and the gas temperature in the immediate vicinity of the droplet surface is the same as in the rest of the cell [1, 37]. The droplet heating in this case is described based

model described in [67]. The latter model is based on an approach which differs from the one used in [52]. One of the main limitations of the model described in [52] is that it was based on the assumption that initially gas temperature was homogeneous in the whole domain. This imposes a serious limitation for practical applications of this model in a realistic environment when the ambient temperature can vary with time.

Near-critical and supercritical droplet heating and evaporation was covered in relatively recent reviews [68, 69], and [64]. Analysis of the interaction between droplets, collisions, coalescence, atomization, oscillations (including instabilities of evaporating droplets) and size distribution were considered in [70{85]). The problem of heating and evaporation of droplets on heated surfaces was considered in [82, 86]. The problem of droplet heating and evaporation is related to spray combustion (see [9, 10, 87{89]). Two groups of models for radiative heating of droplets have been considered: the one based on the assumption that droplets are opaque grey spheres [42, 47, 90], and the one based on the assumption that droplets are semi-transparent for thermal radiation [91{97]. The first approach is the one used in all CFD codes which are known to us, while the second one is much more appropriate from the point of view of underlying physics. The Soret effect describes the flow of matter caused by a temperature gradient (thermal diffusion), while the Dufour effect describes the flow of heat caused by concentration gradients. The two effects occur simultaneously. Both effects are believed to be small in most cases although sometimes their contribution may be significant (see [98{102]). Kinetic and molecular dynamics effects on droplet heating and evaporation were considered in [2{5, 7, 103, 104]. All effects mentioned in this paragraph will be ignored in our analysis.

### 1.3 Structure of the thesis

In Chapter 2 a model for mono-component droplet heating and evaporation, based on the assumption that droplet radius is a linear function of time during time steps, is presented and discussed. A more general model, based on the assumption that droplet radius is an a priori known function of time, is discussed in Chapter 3.

In Chapter 4 the effects of the moving boundary on the solution to the species diffusion equation in multi-component droplets are discussed. A model for body heating/cooling, when this body is immersed into an ambient gas with temperature

# Chapter 2

## Transient heating of an evaporating droplet when droplet is a linear function of time

### 2.1 Introduction of Chapter 2

Taking into account the effect of receding droplet radius on droplet heating and evaporation leads to the well known Stefan problem, which has been widely discussed in the literature (e.g. [105]-[54]), but has been rarely applied to engineering sprays, due to the complex structure. Hence, a substantial gap has developed between mathematical and engineering research in this field. The main objective of this work is to fill this particular gap. This will include the development of an appropriate mathematical model for specific spray applications, and the actual application of this model to simulate droplet heating and evaporation processes in Diesel engine-like conditions. There has been no previous research in this direction to the best of our knowledge.

The essence of the difference between the new approach to the modelling of droplet heating and evaporation, suggested in this chapter, and the traditional approach is schematically illustrated in Fig. 2.1. As follows from this figure, the approximation of the reduction of the droplet radius during the time step by the linear function is noticeably much more accurate than the approximation based on the assumption that the droplet radius is constant during the time step (the conventional approach



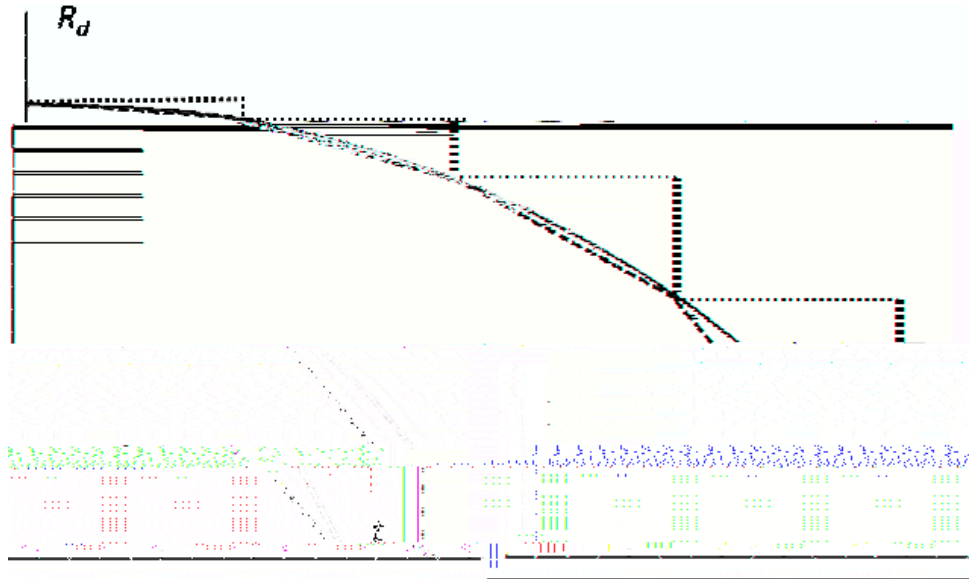


Figure 2.1: A schematic presentation of the plot  $R_d$  versus  $t$  for an evaporating droplet (solid); approximation of this plot using the conventional approach assuming that  $R_d = \text{const}$  during the time step (dotted); approximation of this plot using the new approach assuming that  $R_d$  is the linear function of  $t$  during each time step (dashed).

used in CFD codes). This difference, however, can be mitigated by choosing sufficiently small time steps (more time steps would be required in the case when the reduction of droplet radius during the time step is ignored than in the case when it is taken into account). A more important implication of the new approach, compared with the traditional one, however, is that the effect of the reduction of droplet radius on droplet heating is explicitly taken into account in the new approach at every time step. This leads to the prediction of temperatures different compared with the ones predicted by the traditional approach, regardless of how many time steps are used in the analysis. These differences in droplet temperatures lead to different time dependencies of droplet radii. These effects will be illustrated in this chapter using examples of fuel droplet heating and evaporation in Diesel engine-like conditions.

The basic equations and approximations of the new model are described in Section 2. The analysis and solutions of these basic equations are given in Section 3. In Section 4, one of these solutions is analysed for the values of parameters typical for Diesel engines. The main results of the chapter are summarised in Section 5.

## 2.2 Basic equations and approximations

Let us assume that an evaporating droplet is immersed into a homogeneous hot gas at constant temperature  $T_g$ . The droplet is heated by convection, with the convection heat transfer coefficient  $h(t)$  depending on time  $t$  and droplet radius  $R_d(t)$ , and cools down due to evaporation.  $R_d(t)$  is a continuously differentiable function of time in the range  $0 \leq t \leq t_e$ , where  $t_e$  is the evaporation time. Both  $R_d(t)$  and  $h(t)$  are assumed to be known. Effects of thermal radiation are taken into account. The changes in the droplet temperature ( $T = T(t; R)$ ) are described by the heat conduction equation in the form [105, 106]:

$$\frac{\partial T}{\partial t} = \frac{\partial^2 T}{\partial R^2} + \frac{2}{R} \frac{\partial T}{\partial R} + P(R) \quad (2.1)$$

for  $0 \leq t < t_e$ ,  $0 \leq R < R_d(t)$ , where  $\kappa_l$  is liquid thermal diffusivity ( $\kappa_l = k_l / (\rho_l c_l) = \text{const}$ ),  $k_l$  is the liquid thermal conductivity,  $c_l$  is the liquid specific heat capacity,  $\rho_l$  is the liquid density,  $R$  is the distance from the centre of the droplet.

The term  $P(R)$  takes into account the effects of thermal radiation, assuming that droplets are semi-transparent (radiation can penetrate inside droplets). Various approximations for  $P(R)$  were suggested in [91][107].

Remembering the physical background of the problem, we look for the solution of this equation in the form of a twice continuously differentiable function  $T = T(t; R)$  for  $0 \leq t < t_e$ ,  $0 \leq R < R_d(t)$ . This solution should satisfy the boundary condition:

$$\kappa_l \frac{\partial T}{\partial R} + hT \Big|_{R=R_d(t)} = hT_g + \rho_l L R_d(t); \quad (2.2)$$

$T$  is finite and continuous at  $R \rightarrow +0$ ,  $T_s = T(R_d(t); t)$  is the droplet's surface temperature,  $L$  is the specific heat of evaporation. We took into account that  $R_d(t) \frac{dR_d}{dt} \geq 0$ . Effects of swelling are ignored. Equation (2.2) is just the energy balance condition at  $R = R_d(t)$ . The initial condition is taken in the form:

$$T(t = 0) = T_0(R); \quad (2.3)$$

where  $0 \leq R \leq R_{d0} = R_d(t = 0)$ .

The value of  $R_d(t)$  is controlled by fuel vapour diffusion from the droplet surface, and can be found from the equation [1]:

$$R_d = \frac{k_g \ln(1 + B_M)}{\rho_l c_{pg} R_d}; \quad (2.4)$$

where

$$B_M = \frac{Y_{vs} - Y_{v1}}{1 - Y_{vs}}; \quad (2.5)$$

is the Spalding mass transfer number  $Y_{fs}$  is the mass fraction of fuel vapour near the droplet surface:

$$Y_{fs} = 1 + \frac{p}{p_{fs}} \left( 1 - \frac{M_a}{M_f} \right); \quad (2.6)$$

$Y_{v1}$  is the mass fraction of fuel vapour in ambient gas (in our analysis we assume  $Y_{v1} = 0$ ),

$p$  and  $p_{fs}$  are ambient pressure and the pressure of saturated fuel vapour near the surface of the droplet respectively,  $M_a$  and  $M_f$  are molar masses of air and fuel;  $p_{fs}$  is calculated from the Clausius-Clapeyron equation presented in the form:

$$p_{fs} = \exp \left[ a - \frac{b}{T_s} \right]; \quad (2.7)$$

$a$  and  $b$  are constants to be specified for specific fuels,  $T_s$  is the surface temperature of fuel droplets in K;  $p_{fs}$  predicted by Equation (2.7) is in kPa.

In [15] it was assumed that  $R_d = \text{const}$ , while the contribution of  $R_d$  was taken into account by replacing gas temperature with the so called effective temperature. It was assumed that this approach is applicable when used during relatively short times (time steps in computational fluid dynamics (CFD) codes), but it has never been rigorously justified. The focus of this chapter is on the effects of changing droplet radius during the time step on the heating of droplets.

The current state of the development of mathematical tools for the solution of this type of problem is described by Kartashov [105]. In the following analysis, some of the results described in [105] will be adapted to the investigation of our problem.

A number of simplifying assumptions will be made. Firstly, the contribution of thermal radiation will be ignored ( $P(R) = 0$ ). Secondly, we assume that  $R_d(t)$  is the linear function of  $t$ :

$$R_d(t) = R_{d0} + \dot{R}_d t$$

108]. As follows from the analysis of [96], in the case when external temperature, responsible for radiative heating, is about or less than 1000 K the effect of radiation on droplet evaporation is less than about 1% (see Fig. 2.3 of [96]). This justifies our assumption that  $P(R) = 0$ .

The second assumption is justified if the results are applied to a relatively short period of time, when  $R_d(t)$  can be expanded into a Taylor series in time and only the first two terms are retained (in our previous analyses and in all CFD codes known to us, only the zeroth terms were used). In this case,  $t = 0$  will refer to the beginning of the time step  $t_0$ ,  $t_e$  will refer to  $t_0 + \Delta t$ , where  $\Delta t$  is the time step.

Note that Brenn [54], considering a different problem of calculating the concentration field in evaporating droplets, assumed that  $R_d^2$ , rather than  $R_d$ , is a linear function of time during the whole evaporation process:

$$R_d^2(t) = R_{d0}^2 + \theta t. \quad (2.10)$$

This could be justified by Eq. (2.4) assuming that  $B_M = \text{const}$ . In our case this assumption can be made during the time step but not during the whole evaporation process. For sufficiently small time steps, both approaches lead to identical results since:

$$R_d = R_{d0} \sqrt{1 + \frac{\theta t}{R_{d0}^2}} \approx R_{d0} (1 + \frac{\theta t}{2R_{d0}^2});$$

where  $\theta = \frac{2q}{R_{d0}^2}$ .

The problem considered in [54] is more general compared with the one considered in this chapter, as the 3D effects on species concentrations were taken into account in that paper. If only the radial dependence of this concentration is taken into account, Eq. (1) of [54] would have exactly the same structure as Eq. (2.1) in this chapter. However, the solution of his equation cannot be used for our equation due to different boundary conditions used in our papers.

Among other assumptions used in our analysis we mention that the effects of the interaction between droplets were ignored. This can be justified when the distance parameter (ratio of the distance between droplets to their diameters) is large (see [49] for details).

## 2.3 Analysis of the equations

### 2.3.1 Preliminary analysis

Let us rewrite boundary condition (2.2) in the form:

$$\frac{\partial T}{\partial R} + h$$

we can rewrite Equation (2.12) as

$$R_d^2(t)F_t^0 = F^{00} + R_d^0(t)R_d(t)F^0: \quad (2.16)$$

Equation (2.16) is identical to the one studied in [109], where the distribution of temperature in the melting region was considered (plane problem).

Equation (2.16) is to be solved at  $t \geq [0; t_e]$  (or  $t \geq [t_0; t_0 + \tau]$ ) and  $0 \leq x \leq 1$ . Initial and boundary conditions for this equation can be presented as:

$$F|_{t=0} = R_{d0} T_0(R_{d0}); \quad 0 \leq x \leq 1;$$

$$F|_{x=0} = 0; \quad F + H(t)F_x|_{x=1} = \tilde{v}(t); \quad 0 \leq t \leq t_e \text{ (or } t \geq [t_0; t_0 + \tau]);$$

where  $H(t) = H(t)R_d(t)$ ,  $\tilde{v}(t) = M(t)R_d^2(t)$ .

Following Kartashov [105], we introduce the new unknown function  $W(t; x)$  via the relation:

$$F(t; x) = \alpha \frac{1}{R_d(t)} \exp \left[ -\frac{R_d^0(t)R_d(t)}{4} x^2 \right] W(t; x); \quad (2.17)$$

From Equation (2.17) we obtain the following expressions for the derivatives:

$$F_t^0 = \left( \frac{1}{2} R_d^{3=2}(t) R_d^0(t) + R_d^{1=2}(t) \frac{(R_d^0(t))^2 + R_d(t) R_d^{00}(t)}{4} \right) W(t; x) + R_d^{1=2}(t) W_t^0(t; x) \exp \left[ -\frac{R_d^0(t)R_d(t)}{4} x^2 \right];$$

$$F^0 = \left( \frac{2}{4} \frac{R_d^0(t)R_d(t)}{R_d(t)} W(t; x) + \alpha \frac{1}{R_d(t)} W^0(t; x) \right) \exp \left[ -\frac{R_d^0(t)R_d(t)}{4} x^2 \right];$$

$$F^{00} = \alpha \frac{2}{R_d(t)} \frac{R_d(t)R_d^0(t)}{4}$$

In the case of non-zero  $\frac{d^2 R_d}{dt^2}$  and  $P(R)$ , Eq. (2.18) would need to be replaced by the following equation (cf. Equation (8.149) in [105]):

$$R_d^2(t)W_t^0(t; ) = W^{00}(t; ) + \frac{1}{4} \frac{d^2 R_d}{dt^2} W(t; ) + \frac{R_d^2 R}{\alpha_k( ; t)} P(R); \quad (2.19)$$

where

$$\alpha_k( ; t) = \frac{1}{R_d(t)} \exp \left[ \frac{R_d^0(t) R_d(t)}{4} \right];$$

Equation (2.19) reduces to Equation (2.18) in the limit when  $\frac{d^2 R_d}{dt^2} = 0$  and  $P(R) = 0$ .

Equation (2.18) is to be solved subject to initial and boundary conditions:

$$W(t; )|_{t=0} = W_0($$





The solution to Equation (2.28) gives a set of positive eigenvalues  $\lambda_n$  numbered in ascending order ( $n = 1; 2; \dots$ ). If  $h_0 = 0$ , then  $\lambda_n = (n - \frac{1}{2})^2$ . Assuming that  $B = 1$ , expressions for eigenfunctions  $v_n(x)$  can be written as:

$$v_n(x) = \sin \lambda_n x \quad (n = 1; 2; \dots); \quad (2.29)$$

The solution  $\lambda = 0$  is excluded as it leads to a trivial solution  $v_n(x) = 0$ .

The value of  $B$  is implicitly accounted for by the coefficients  $a_n(t)$  in Series (2.25). The functions  $v_n(x)$  form a full set of eigenfunction functions which are orthogonal for  $x \in [0; 1]$ . The orthogonality of functions  $v_n(x)$  follows from the relation:

$$\int_0^1 v_n(x) v_m(x) dx = \delta_{nm} \int_0^1 v_n^2(x) dx; \quad (2.30)$$

where:

$$\delta_{nm} =$$

this case one can show that [15]:

$$|q_n| < \frac{\text{const}}{n^2} \quad (2.34)$$

Remembering Equations (2.25) and (2.32), Equation (2.24) can be rewritten as:

$$\sum_{n=1}^{\infty} R_d^2(t) \frac{d}{dt} \frac{n(t)}{n^2} + n(t) \frac{1}{n^2} v_n(\cdot) = \sum_{n=1}^{\infty} f_n R_d^2(t) \frac{d}{dt} \frac{o(t)}{n^2} + v_n(\cdot) \quad (2.35)$$

Both sides of Equation (2.35) are Fourier series with respect to functions  $v_n(\cdot)$ . Two Fourier series are equal if, and only if, their coefficients are equal. This implies that:

$$R_d^2(t) \frac{d}{dt} \frac{n(t)}{n^2} + n(t) \frac{1}{n^2} = f_n R_d^2(t) \frac{d}{dt} \frac{o(t)}{n^2} \quad (2.36)$$

Equation (2.36) is to be solved subject to the initial condition:

$$n(0) = q_n + o(0) f_n \quad (2.37)$$

To simplify the notation, hence-forward it is assumed that  $t_0 = 0$ .

The general solution to the homogeneous equation:

$$R_d^2(t) \frac{d}{dt} \frac{n(t)}{n^2} + n(t) \frac{1}{n^2} = 0 \quad (2.38)$$

can be presented as:

$$\ln \left( \frac{n}{n_0} \right) = - \int_0^t \frac{1}{R_d^2(\tau)} d\tau$$

$$\exp \left[ -\frac{2}{R_{d0} R_d(t)} \int_0^t \frac{1}{R_d(\tau)} d\tau \right] n(0) \exp \left[ -\frac{2}{R_{d0} R_d(t)} \int_0^t \frac{1}{R_d(\tau)} d\tau \right] : \quad (2.42)$$

Remembering Equations (2.40) and (2.41), the solution to Equation (2.36) can be presented as:

$$n(t) = n(0) \exp \left[ -\frac{2}{R_{d0}^2} \int_0^t \frac{1}{1+\tau} d\tau \right] + f_n \int_0^t \frac{1}{d} \exp \left[ -\frac{2}{R_{d0}^2} \int_0^t \frac{1}{1+\tau} d\tau \right] d\tau : \quad (2.43)$$

Remembering (2.42) and (2.37) we can write an alternative formula for  $n(t)$ :

$$n(t) = q_n \exp \left[ -\frac{2}{R_{d0} R_d(t)} \int_0^t \frac{1}{R_d(\tau)} d\tau \right] + f_n \int_0^t \frac{1}{R_d(\tau)} \exp \left[ -\frac{2}{R_{d0} R_d(t)} \int_0^t \frac{1}{R_d(\tau)} d\tau \right] d\tau : \quad (2.44)$$

Note that  $n(t)$  in the form (2.43) satisfies Equation (2.36), while  $n(t)$  in the

where  $\rho_n$  are given by Equations (2.43) or (2.44).

Note that strictly speaking Equation (2.45) is an implicit function of droplet temperature since  $\rho_n$  depends on droplet surface temperature  $T_s$  (see Fig. 2.2). Hence, the iteration process would be required. However, as follows from our calculations (see Figs. 2.2 and 2.4-2.6), except at the very final stage of droplet evaporation, for sufficiently small time steps, the value of  $T_s$  can be taken equal to the one obtained at the end of the previous time step. This allows us to consider Equation (2.45) as an explicit formula for  $T(R)$ .

### 2.3.3 Analysis of the general case

Let us now relax our assumption that  $H_0(t) = h_0 = \text{const} > 1$  and assume that:

$$H_0(t) = h_0 + h_1(t); \quad (2.46)$$

where  $h_0 = \text{const} > 1$ . Note that many of the following equations would be greatly simplified in the case when  $h_0 = 0$ . In view of (2.46) we can rewrite the boundary condition at  $r = 1$  for Equation (2.18) in the form:

$$\left. \frac{\partial W}{\partial r} \right|_{r=1} + h_0 W(t; 1) = h_0(t) + h_1(t) W(t; 1) - \hat{\rho}_0(t); \quad (2.47)$$

Assuming that  $\hat{\rho}_0(t)$  is known, we can formally use the previously obtained

$$G(t; \tau) = \sum_{n=1}^{\infty} \sin(n\tau) \frac{\sin(n t)}{R_d^2(\tau) \int \int v_n \int \int^2} \exp \left[ -\frac{2}{R_{d0}} \frac{1}{R_d(t)} \frac{1}{R_d(\tau)} \right] ;$$

Explicit expressions for  $f_n$  have been used in these formulae. Both functions  $V(t; \tau)$  and  $G(t; \tau)$  are assumed to be known.

Remembering (2.47), we can rewrite Equation (2.49) as:

$$W(t; \tau) = V(t; \tau) + \int_0^t [h_0(s) + h_1(s)W(s; \tau)] G(t; \tau) ds ; \quad (2.50)$$

This is an integral representation for a solution to Problem (2.18)-(2.22) for time dependent  $H_0(t)$  given by Equation (2.46). For  $\tau = 1$ , integral representation (2.50) reduces to the Volterra integral equation of the second kind for function  $W(t; 1)$ :

$$W(t; 1) = V(t; 1) + \int_0^t [h_0(s) + h_1(s)W(s; 1)] G(t; 1) ds ;$$

Once the solution to this equation has been found we can substitute it into integral representation (2.50) and find the required solution to the initial and boundary value problem (2.18) { (2.22). The required distribution of  $T$  is found to be:

$$T(t; R) = \frac{1}{R} \frac{1}{R_d(t)} \exp \left[ -\frac{R_d^0(t) R^2}{4 R_d(t)} \right] W(t; R=R_d(t)); \quad (2.56)$$

In the case when  $h_1(t) = 0$  and  $t \rightarrow 1$  this solution reduces to that given by Equation (16) of [15]. Note that in the case of  $h_0 = 0$  we have  $n = (n - 1 = 2)$  and  $jjV_njj^2 = 1 = 2$  in all equations.

## 2.4 Analysis of the solutions

As follows from the previous analysis, the importance of the effects described by the new model depends on the value of the coefficient given by Equation (2.9). The plots of versus droplet surface temperature  $T_s$

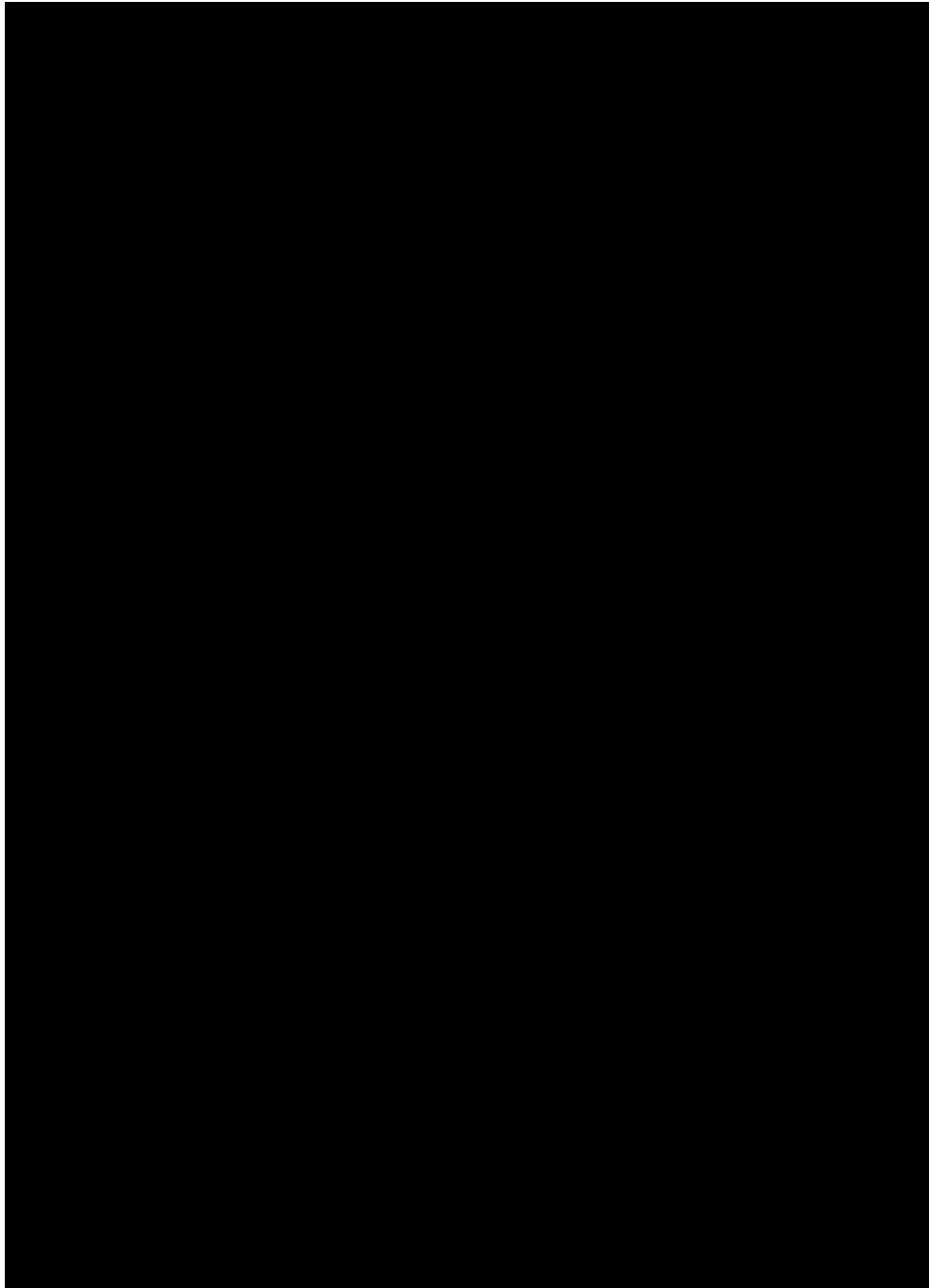


Figure 2.2: The plots of  $\dots$  versus droplet surface temperature  $T_s$  for  $M_a = 29$  kg/kmole,  $M_f = 170$  kg/kmole ( $C_{12}$ )

have performed similar calculations but for  $T_g = 2000$  K (not shown). The plots without evaporation for  $R_{d0} = 50$  nm in this case coincided with the ones shown in Fig. 2.2 of [15], obtained using the conventional approach.

In Fig. 2.4 we compared the results of calculations of droplet surface temperatures, taking into account the ev



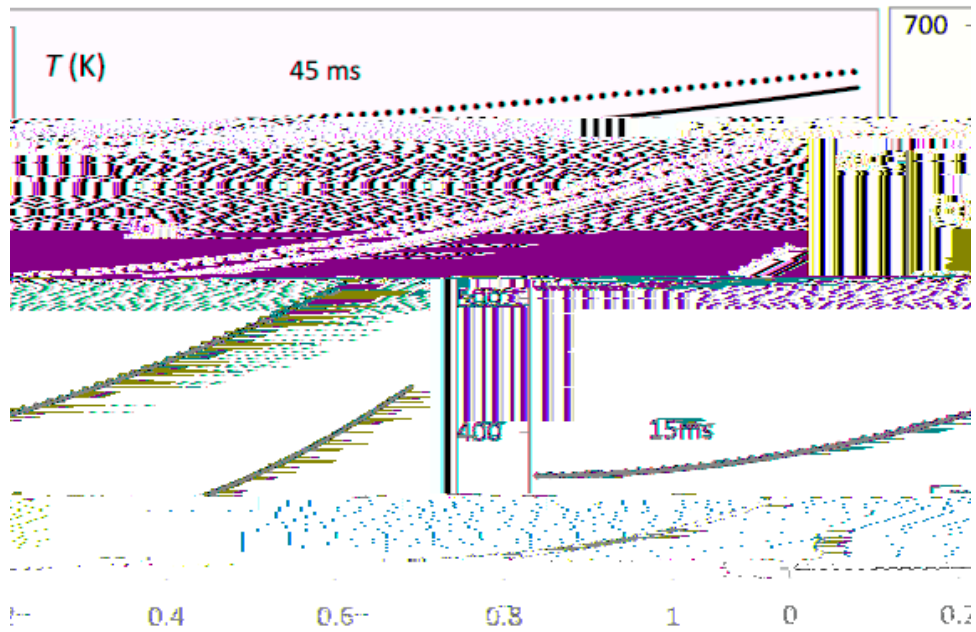
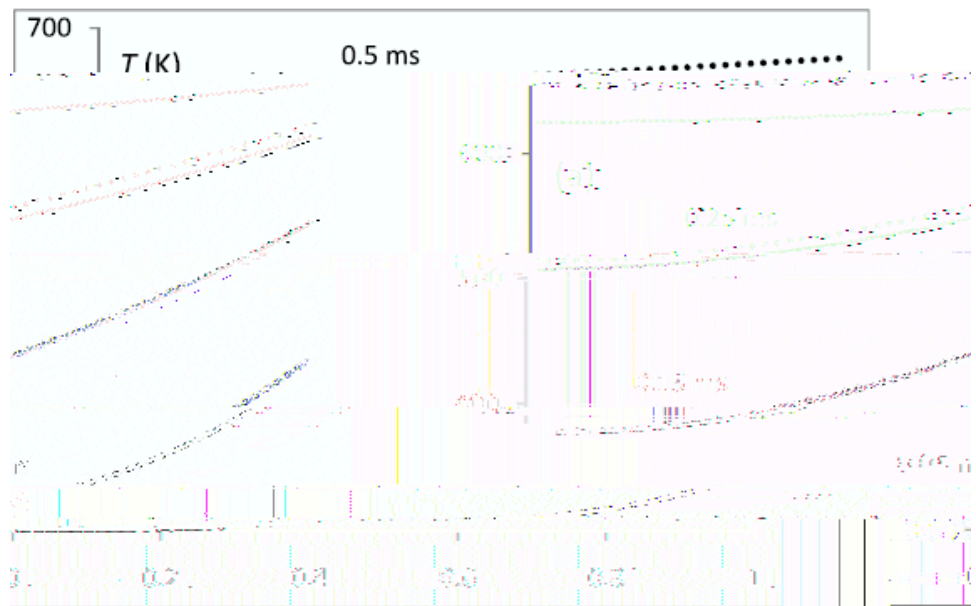


Figure 2.3: The plots of  $T$  versus  $R = R_d$  for the same values of parameters

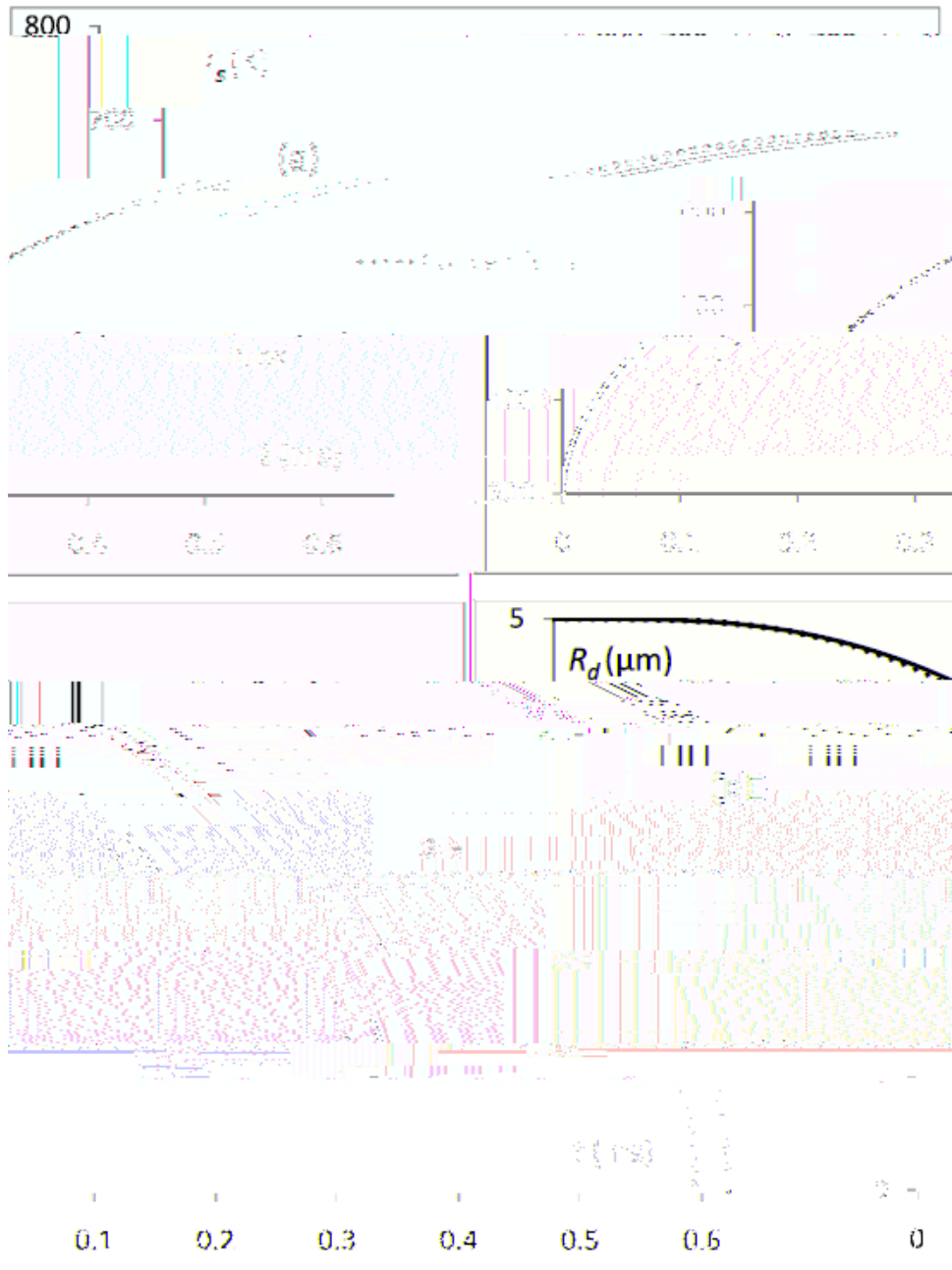


Figure 2.4: The plots of  $T_s$  versus time (a) and  $R_d$  versus time (b) for heated and evaporating droplets using the conventional (dotted), and new (solid) approaches for  $T_g = 1000$  K and  $R_{d0} = 5 \mu\text{m}$ .

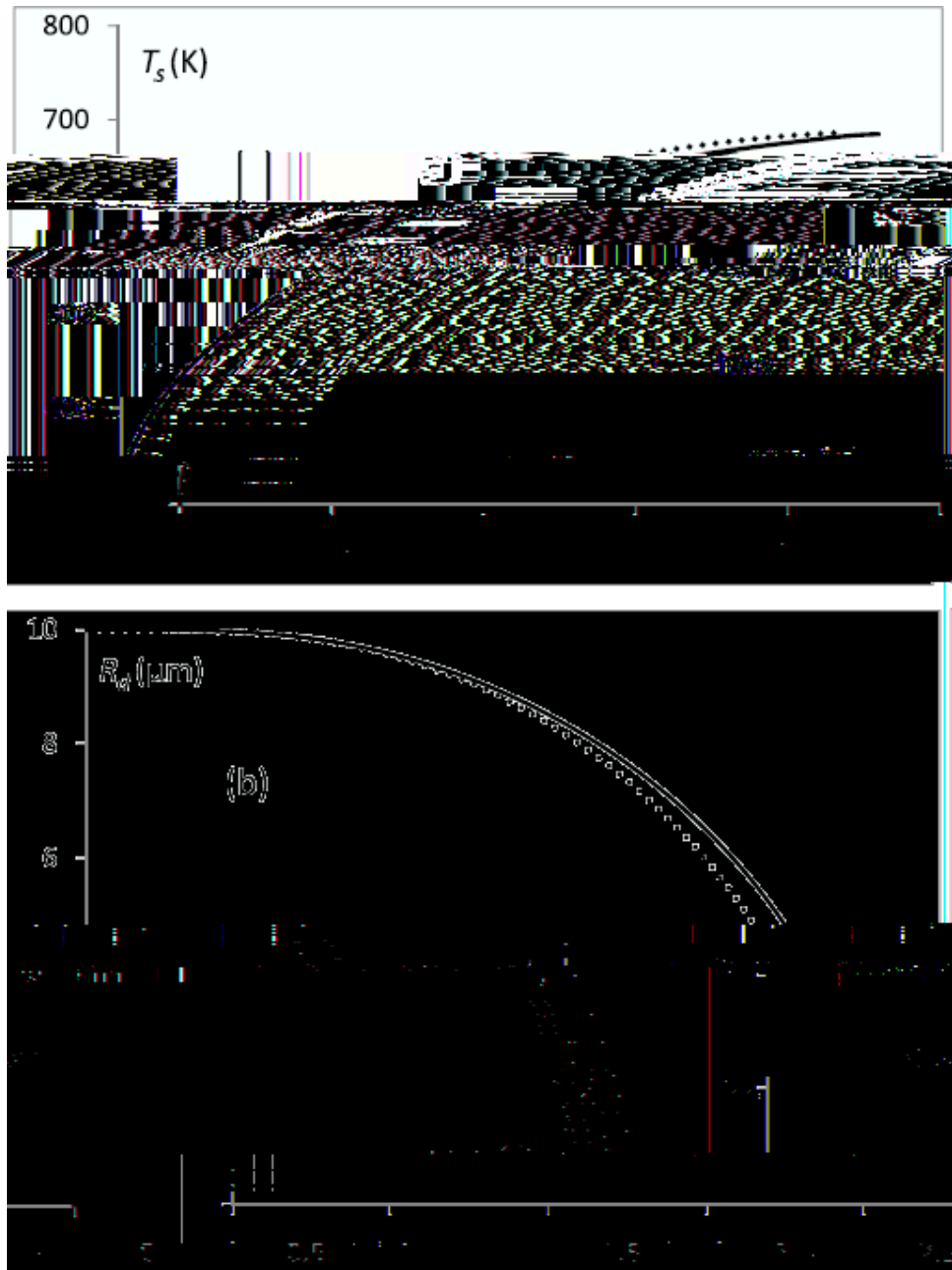


Figure 2.5: The same as Fig. 2.4 but for  $R_{d0} = 10 \text{ m}$ .

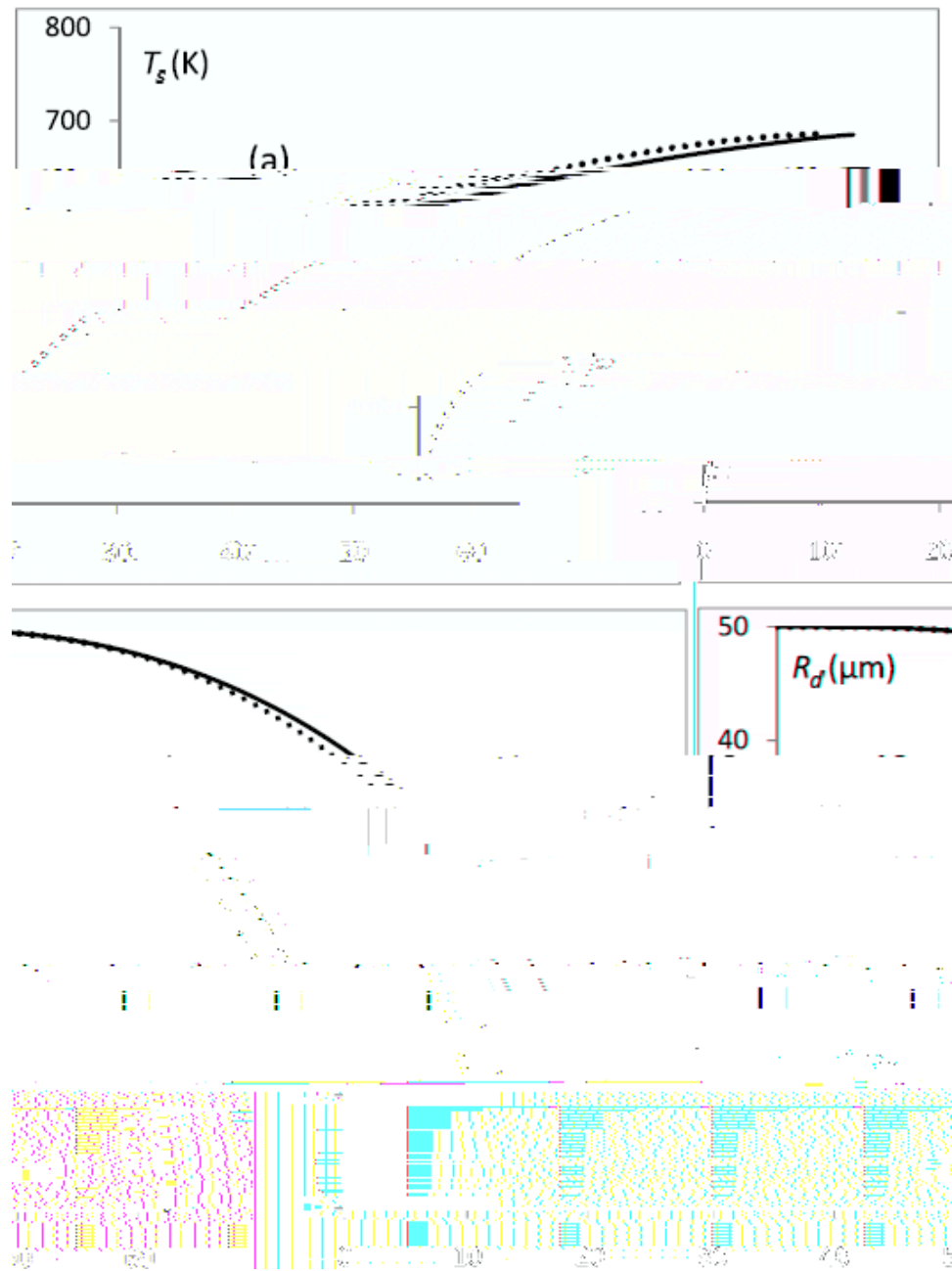
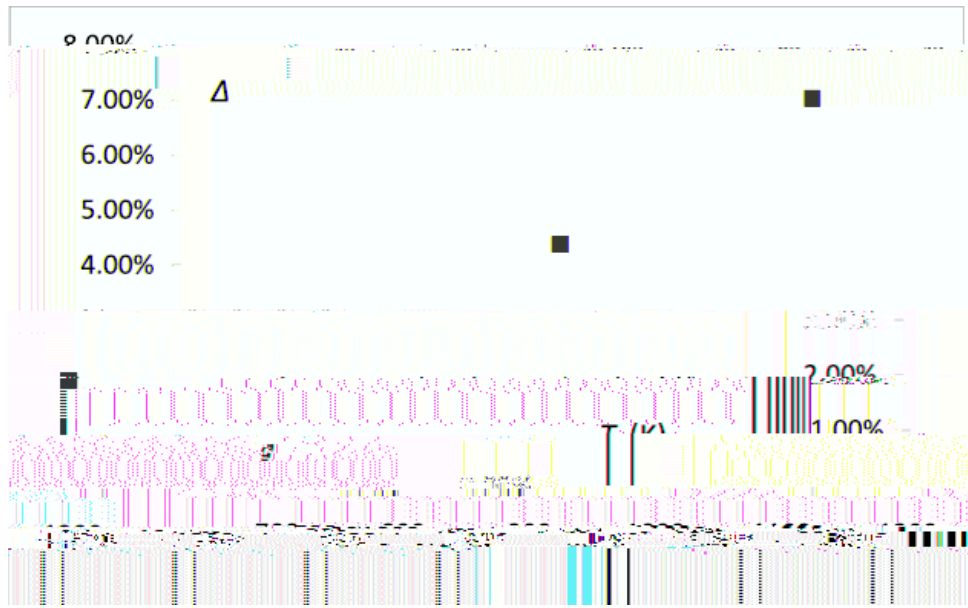


Figure 2.6: The same as Fig. 2.4 but for  $R_{d0} = 50 \mu\text{m}$ .





To compare results obtained using different methods dimensionless variables are used:  $\mathcal{R} = \frac{R_d}{R_{d0}}$  ;  $s = \frac{T_s - T_0}{T}$

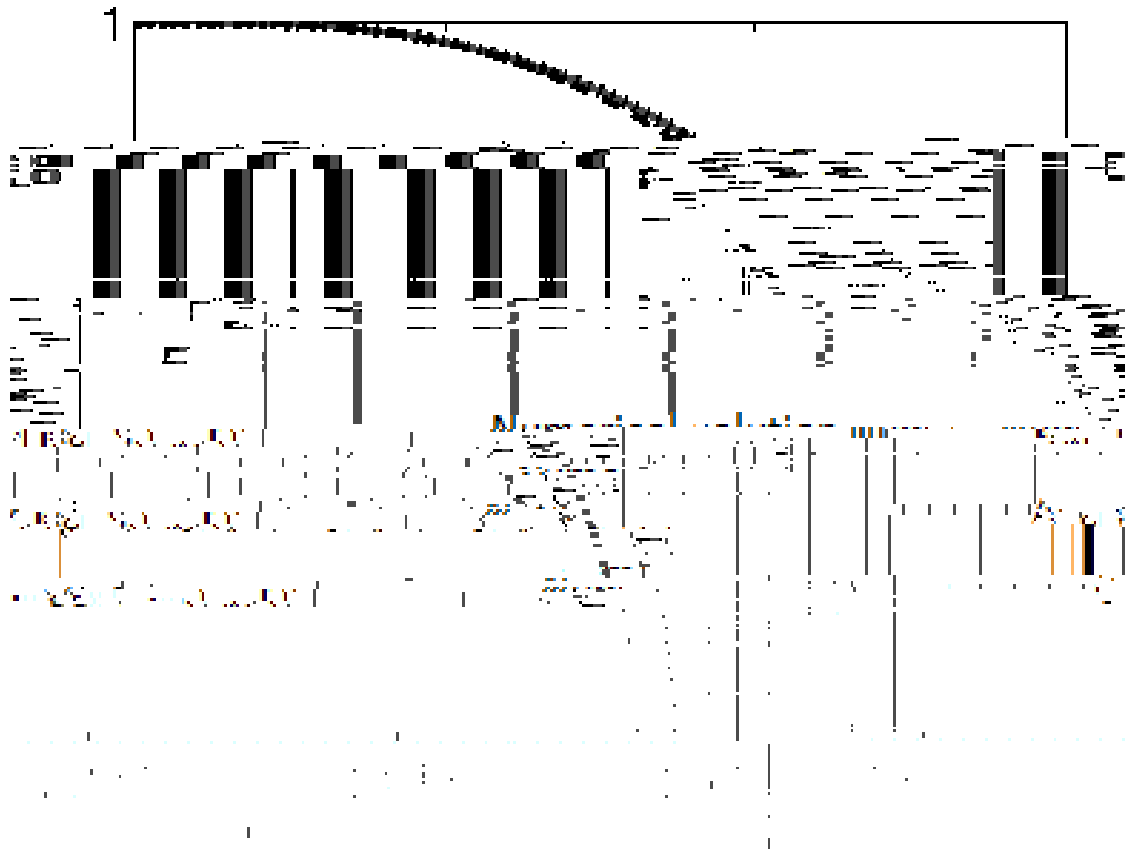


Figure 2.10: Comparison of  $R$  vs.  $t$  obtained using three different methods: the box scheme (solid); the method developed in this chapter (dotted); and the conventional method for which  $R(t)$  is piecewise constant in time (dashed).

the result obtained, assuming that  $R(t)$  is piecewise constant in time, and the results taking into account the changes of  $R(t)$  during time steps. The results predicted by the numerical solution coincides within the accuracy of plotting with the one predicted by the model described in this chapter (as in the case shown in Fig. 2.9).

It is indicated in [23] that, for given values of  $T_0$  and  $T_g$ , the maximum surface temperature reached is always the same, regardless of the initial droplet radius. Note that this maximal temperature (wet-bulb temperature) is asymptotically approached only in the case when the contribution of thermal radiation is ignored; when this contribution is taken into account, the droplet temperature reaches its maximal temperature, which is greater than the wet-bulb temperature, and then decreases, approaching the wet-bulb temperature from above [44]. Fortunately, for the case of



negligible thermal radiation, we are able to investigate this further analytically, as shown in [23]. In brief, an analytical solution can be found at  $t_e$ ; and from this we





### 3.2 Solution for the case of arbitrary $R_d(t)$ but $T_{\infty}(R) = \text{const}$

The analysis of this Chapter is based on the assumption that  $T_{\infty}(R) = T_{\infty} = \text{const}$ . In this case we can introduce the new variable  $v = u - RT_{\infty}$  and rearrange Equation (2.12) as:

$$\frac{\partial v}{\partial t} = \frac{\partial^2 v}{\partial R^2} \quad (3.1)$$

for  $t \geq (0; t_e)$  and  $R \geq (0; R_d(t))$  with the boundary conditions

$$\frac{\partial v}{\partial R} + H(t)v \Big|_{R=R_d(t)} = 0(t); \quad (3.2)$$

$$v|_{R=0} = 0 \quad (3.3)$$

for  $t \geq (0; t_e)$  and the initial condition

$v(t) = 0$  for  $t = 0$  and  $R \in (0; R_d(t))$

- 2) It satisfies Conditions (3.3) and (3.4);
- 3) It is continuous at  $R \neq R$

(cf. Equation (3.9)). Therefore, the integral in Equation (3.10) is defined as an improper integral.

Note that  $G_1(t; R = 0) = 0$ .

Function  $U(t; R)$  has the following properties [105, 130]:

- 1) It satisfies Equation (3.1) for  $0 < t < t_e$  and  $0 < R < R_e$ ;
- 2) It satisfies the boundary Condition (3.3) for  $0 < t < t_e$ ;
- 3) It satisfies the initial condition

$$U(t; R)|_{t=+0} = \begin{cases} RT_{d0}(R) & \text{when } 0 < R < R_e \\ 0 & \text{when } R > R_e \end{cases} \quad (3.15)$$

The latter relation follows from the property of the delta-function:

$$\lim_{\delta \rightarrow 0} \int_{-\delta}^{\delta} \delta(x) \exp(-x^2/\delta) dx = 1 \quad (3.16)$$

We look for the solution to Equation (2.12) in the form:

$$u(t; R) = U(t; R) + v(t; R) \quad (3.17)$$

Having substituted Equation (3.17) into Equation (2.12) and boundary and initial conditions (2.13) { (2.15), we obtain problem (3.1) { (3.4) for

Hence, we obtain an explicit expression for  $\rho_0(t)$  in the form:

$$\begin{aligned} \rho_0(t) = & \frac{1}{4^{\rho-1}} \frac{Z_{R_e}}{(t)^{3-2\rho}} \left( T_{d0}(\cdot) \right) \exp \left( \frac{(R_d(t))^2}{4t} \right)^{\#} \\ & \left( R_d(t) + \cdot \right) \exp \left( \frac{(R_d(t) + \cdot)^2}{4t} \right)^{\#} d \\ & \frac{H(t)}{2^{\rho-1} t} Z_{R_e} \left( T_{d0}(\cdot) \right) \exp \left( \frac{(R_d(t))^2}{4t} \right)^{\#} \exp \left( \frac{(R_d(t) + \cdot)^2}{4t} \right)^{\#} d \\ & + M(t)R_d(t): \end{aligned} \quad (3.21)$$

In the limit  $t \rightarrow 0+$  the expression for  $\rho_0(t)$  is simplified to (see Appendix 5):

$$\rho_0(0) = \left( T_{d0}(\cdot) \right)_{=R_{d0}}^{\rho} + H(0)R_{d0}T_{d0}(R_{d0}) + \rho(0): \quad (3.22)$$

Combining Equations (3.5) and (3.17) we can present the final solution to our problem in the form:

$$T(t; R) = \frac{1}{R} U(t; R) + \frac{\rho-}{\text{---}}$$



### 3.4 Implementation of the new solutions into a numerical code

In the solutions presented in the last two sections it was assumed that  $R_d(t)$  is

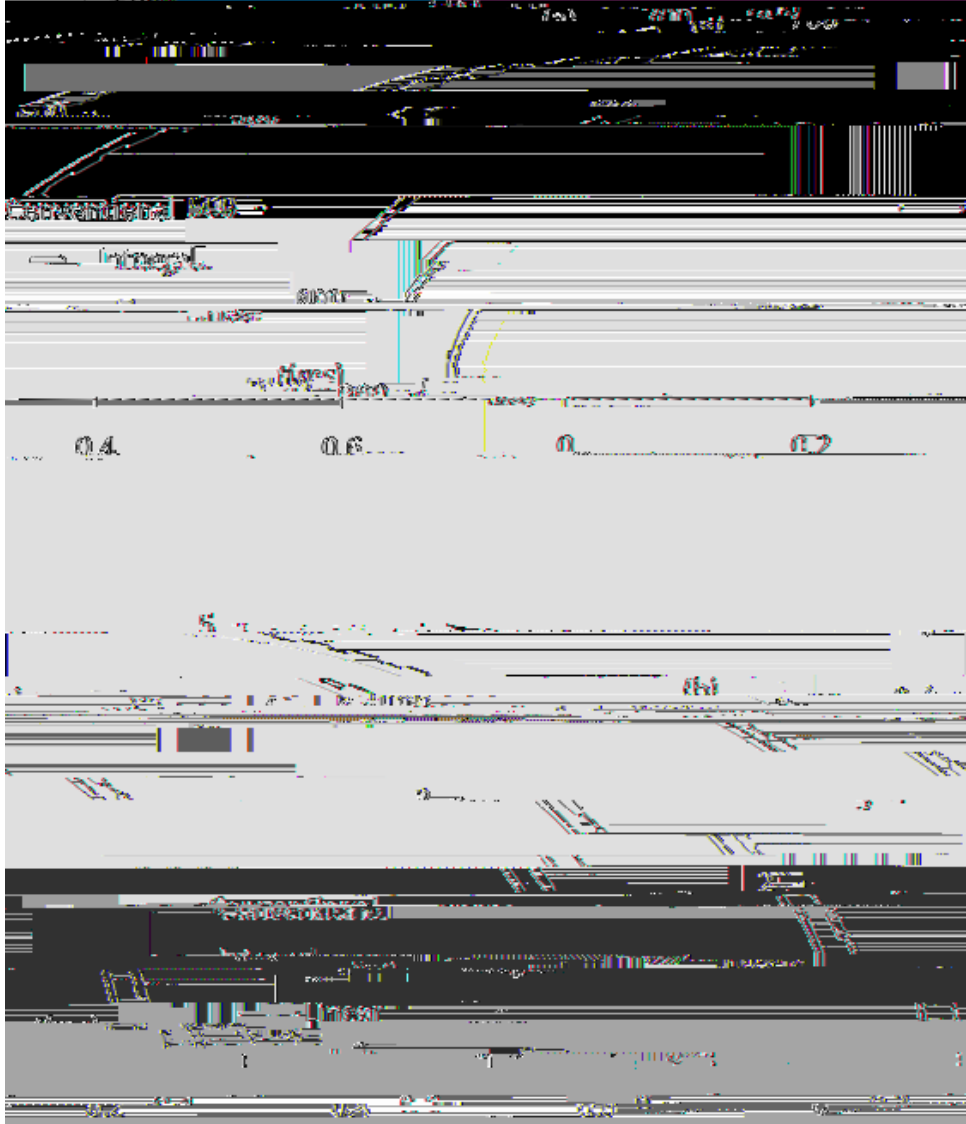


Figure 3.1: The plots of  $T_s$  versus time (a) and  $R_d$  versus time (b) using the conventional model (thick solid), integral model based on Equation (3.11) (dashed) and linear model (thin solid) for a stationary n-dodecane ( $M_f = 170$  kg/kmole) droplet with an initial radius 5  $\mu$ m, evaporating in ambient air at a pressure of  $p = 30$  atm = 3000 kPa and temperature 1000 K.

and linear solution (2.45) practically coincide, which suggests that both approaches are correct and valid. Both these solutions predict lower droplet temperatures and longer evaporation times in agreement with the results reported in previous Chapter. Note that deviations between the predictions of the integral and linear solutions were observed in the immediate vicinity of the time when the droplet completely evaporates.

There were obvious numerical problems when we approached this time due to the fact that the time derivative of  $R_d$  becomes infinitely large. In practice the extrapolation, based on the assumption that the second derivative of  $R_d(t)$  is constant, was used for these times. This leads to small deviations between the predicted evaporation times. In the case shown in Fig. 3.1, the evaporation times predicted by the conventional model, linear solution, and integral solution were 0.595 ms, 0.622 ms and 0.628 ms respectively. That means that the difference between the evaporation times predicted by the linear and integral solutions was less than 1% and can be safely ignored in most practical applications (this error can be reduced further if required). The same comment applies to other cases considered below.

The effect of the choice of the number of iterations on the prediction of the integral solution is illustrated in Fig. 3.2 for the same case as shown in Fig. 3.1. This effect is shown only for the times when the deviation between the results predicted by the linear and integral solutions is maximal. For the first iteration, the time evolution of droplet radius is the same as predicted by the conventional model. The deviation of the corresponding droplet temperatures predicted by the integral and linear solutions appears to be quite noticeable. For the fifth iteration the droplet surface temperatures predicted by the integral and linear solutions practically coincide up to  $t = 0.45$  ms. The corresponding plots of  $R_d(t)$ , predicted by the integral solution, turned out to be closer to those predicted by the linear solution than those predicted by the conventional model. The closeness between the plots predicted by the linear and integral solutions improved as the number of iterations increased. However, even for the 15th iteration the deviation between the results remains visible, although not important for practical applications (cf. Fig. 3.1). For higher iterations the results are practically indistinguishable from those predicted by the 15th iteration. Interestingly, odd iterations predicted smaller  $R_d(t)$  and even iterations

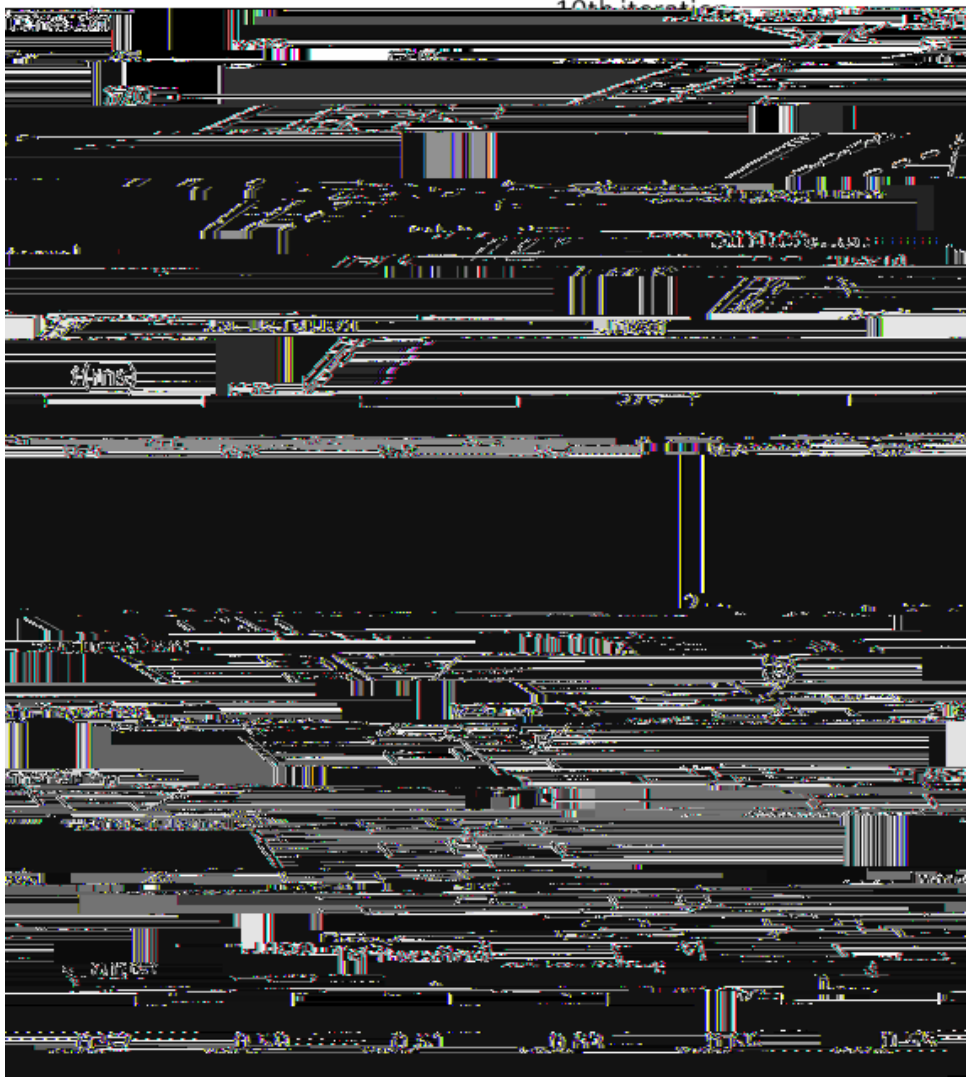


Figure 3.2: The same as Fig. 3.1 but for different numbers of iterations in the integral solution.

predicted larger  $R_d(t)$  compared with those predicted by the linear solution. At the qualitative level this could be related to the fact that a faster evaporation rate, assumed for the first iteration (conventional model), leads to a lower droplet surface temperature. At the second iteration, this lower droplet surface temperature leads to a slower evaporation rate etc.

As to the computational efficiency of the new integral model, we note that for a PC Xeon 3000 Hz (the calculations were processed on one kernel only) with 2357(23))-32B-2

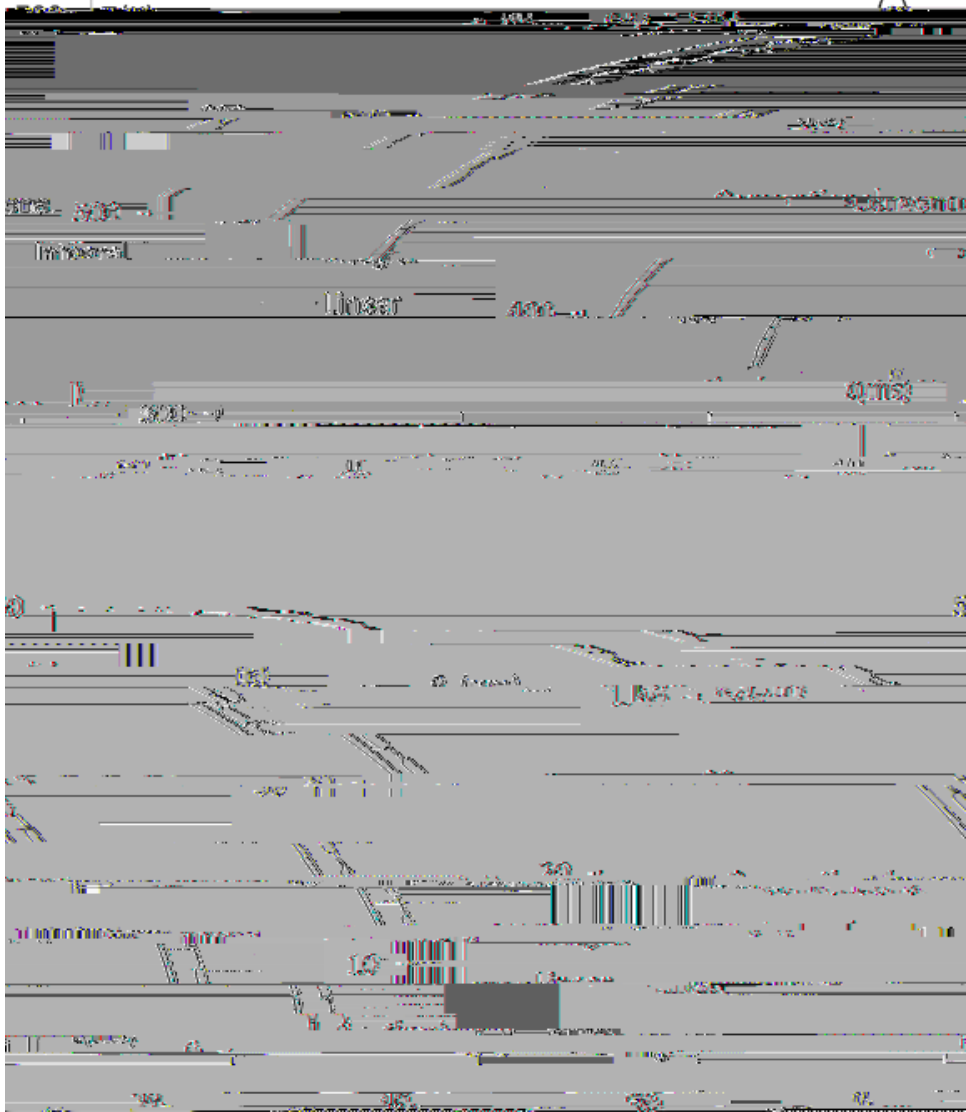


Figure 3.3: The same as Fig. 3.1 but for a droplet with initial radius  $50 \mu\text{m}$ .

computational fluid dynamics (CFD) codes.

The results, similar to those shown in Fig. 3.1, but for droplets with initial radii  $50$  and  $100 \mu\text{m}$  are shown in Figs. 3.3 and 3.4 respectively. As can be seen from these figures, the plots of droplet surface temperatures and radii are largely unaffected by

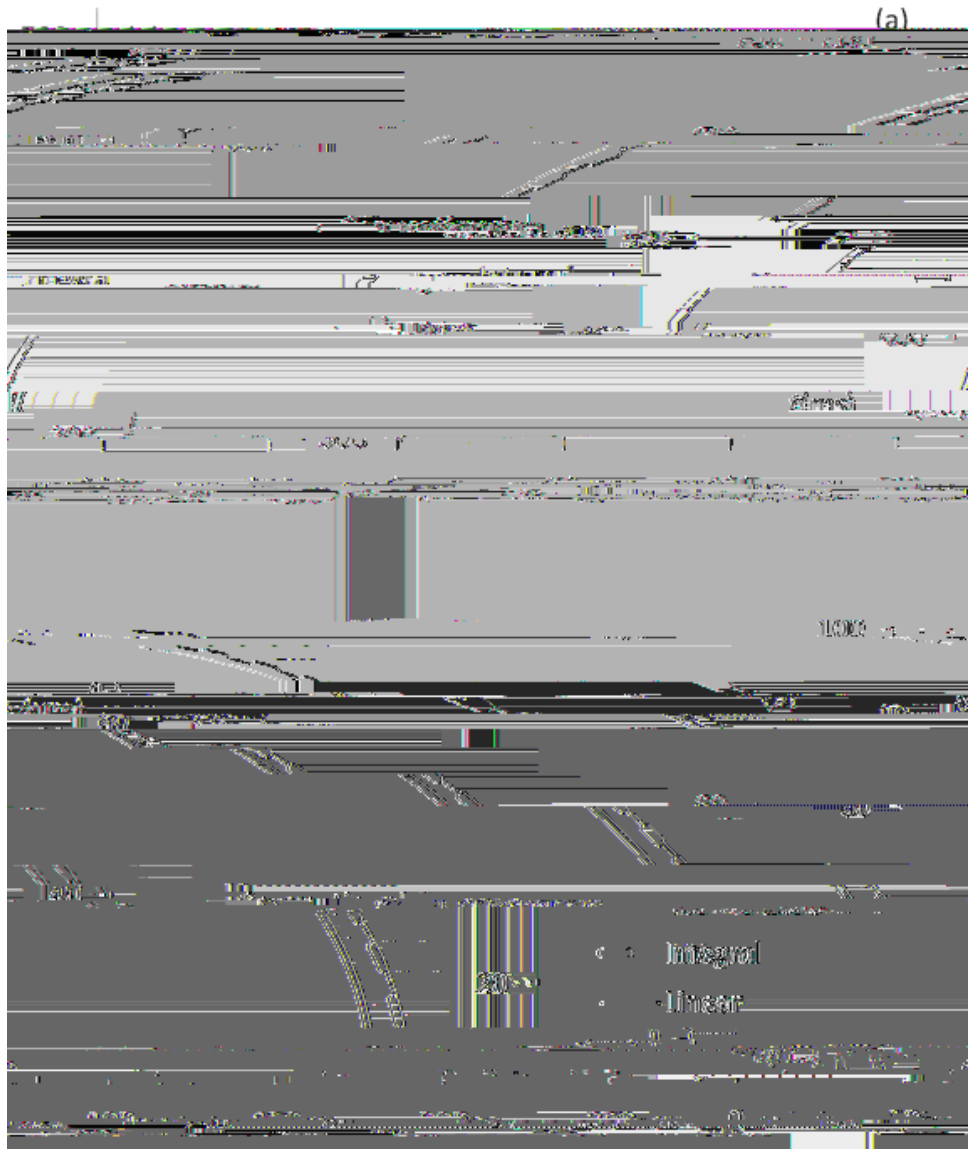


Figure 3.4: The same as Figs. 3.1 and 3.3 but for a droplet with initial radius 100 m.







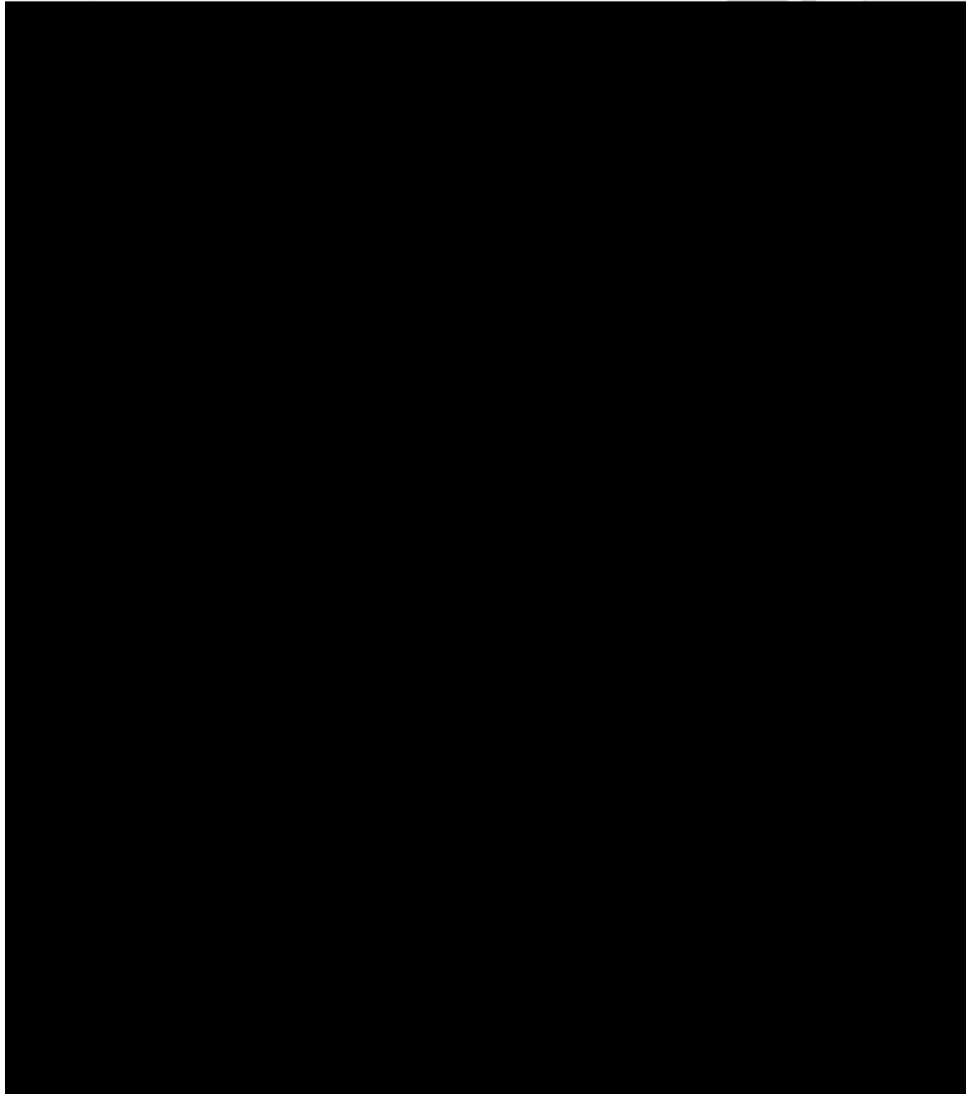


Figure 3.6: The same as Figs. 3.1 and 3.5 but for an ambient gas temperature equal to 1200 K.

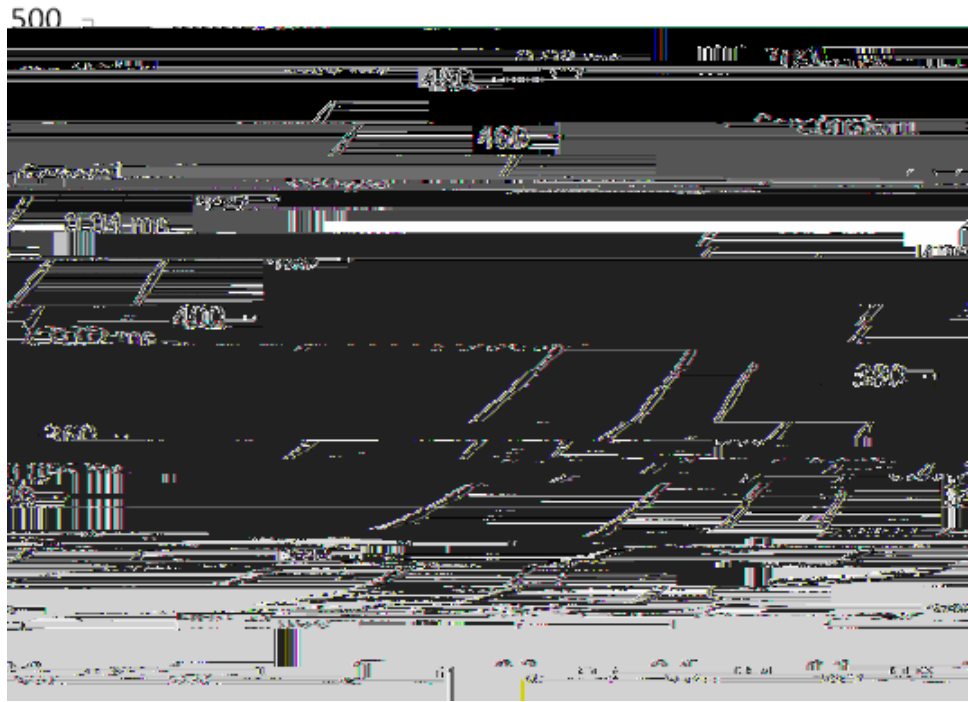


Figure 3.7: The plots of  $T$  versus  $R = R_d$  for a stationary n-dodecane ( $M_f = 170$  kg/kmole) droplet with initial radius  $5 \mu\text{m}$ , evaporating in ambient air

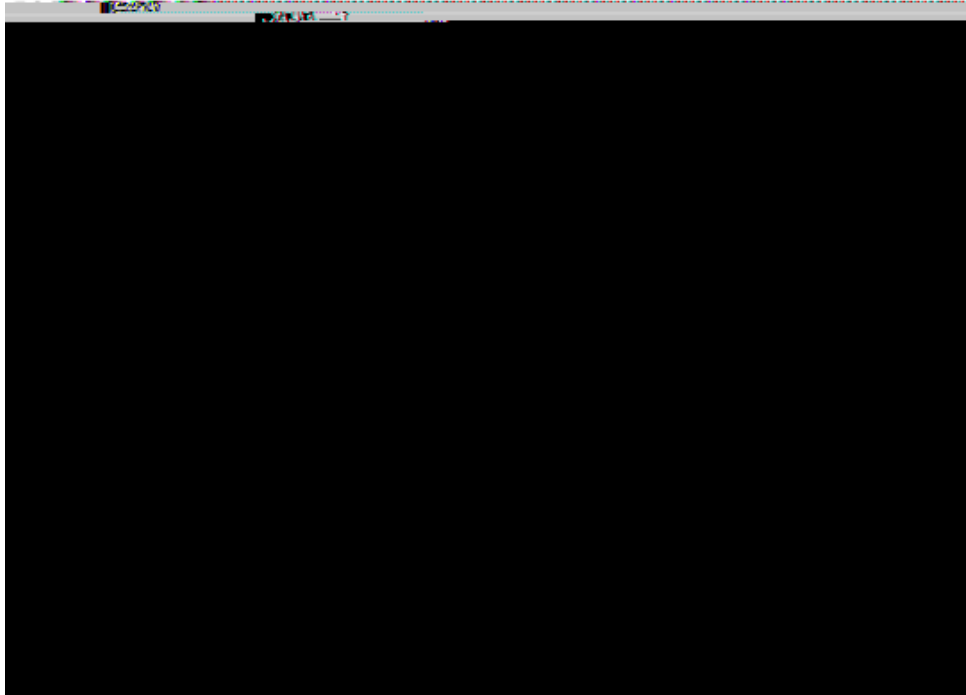


Figure 3.8: The same as Fig. 3.7 but for the general solution (Equation (3.23) applied to the case when the initial distribution of temperature inside the droplet is given by Equation (3.24)).

distribution of droplet temperature was approximated as

$$T_{\infty}(R) = 300 + 10(R/R_{\infty})^2 = 300 + 10(\ )^2; \quad (3.24)$$

and the analysis was based on Equation (3.23).

Comparing the plots referring to both cases, shown in Fig. 3.8, one can see that these plots visibly converge with time. This can be related to the fact that increased droplet surface temperature in the general case leads to decreased convective heating of droplets. Hence the droplet surface temperature increases more slowly in the general case than in the case of constant initial temperature inside droplets.

We appreciate that the errors associated with the conventional assumption that the droplet radii remain constant during the time step can be comparable with or even larger than those associated with other effects, including uncertainties in gas temperature measurements, convection heat transfer coefficient approximations and effect of interactions between droplets in realistic sprays. The importance of the latter effect is discussed in [14, 38], but its analysis lies beyond the scope of this Chapter.

## 3.6 Conclusions of Chapter 3

Two new solutions to the heat conduction equation, describing transient heating of an evaporating droplet, are suggested, assuming that the time evolution of droplet radius  $R_d(t)$  is known. The initial droplet temperature is assumed to be constant or allowed to change with the distance from the droplet centre. The results turned out to be the simplest in the first case and the main focus of our analysis is upon these. Since  $R_d(t)$  depends on the time evolution of the droplet temperature, an iterative process is required. Firstly, the time evolution of  $R_d(t)$  is obtained using the conventional approach, when it remains constant during the time step, but changes from one time step to another. The droplet surface temperature in this case is obtained from the analytical solution of the heat conduction equation inside the droplet. It is assumed that this droplet is heated by convection from the ambient gas, and its radius remains constant during the time step. Then these values of  $R_d(t)$  are used in the new solutions to obtain updated values of time evolution of the distribution of temperatures inside the droplet and on its surface. These new values of droplet temperature are used to update the function  $R_d(t)$ . This process continues until convergence is achieved, which typically takes place after about 15 iterations. The results of the calculations of droplet surface temperature, using this approach, are compared with the results obtained using the previously suggested approach when the droplet radius was assumed to be a linear function of time during individual time steps for typical Diesel engine-like conditions. For sufficiently small time steps the time evolutions of droplet surface temperatures and radii, predicted by both approaches coincide. This suggests that both approaches are correct and valid. Similarly to the case when droplet radius is assumed to be a linear function of time during the time step, the new solution predicts lower droplet temperatures and slower evaporation when the effects of the reduction of  $R_d$  are taken into account.

It is shown that in the case of constant droplet initial temperature, models both taking and not taking into account the changes in initial droplet temperature with the distance from the droplet centre, predict the same results. This suggests that both models are likely to be correct. It is shown that the temperatures predicted by the models based on the assumption of constant initial droplet temperature, and the one taking into account the increase in this temperature with the distance from

the droplet centre, tend to converge with time.

# Chapter 4

## New solutions to the species diffusion equation inside droplets in the presence of the moving boundary

### 4.1 Introduction of Chapter 4

The species diffusion equation, describing the dynamics of multi-component systems, its analysis and applications, has been widely discussed in the literature [53]. One of



and the initial condition  $Y_{li}(t = 0) = Y_{li0}(R)$ , where  $Y_{lis} = Y_{lis}(t)$  are liquid components' mass fractions at the droplet's surface,

$$m = \frac{j m_d j}{4 R_d^2} \quad (4.3)$$

$j$  is the evaporation rate of species.

Note that 0



The latter velocity was calculated as [44]:

$$U_s = 1$$

by correcting the expression for  $Sh_{iso}$  (see [38, 49] for details). This effect is not taken into account in our analysis.

Note that Equation (4.10) is valid for arbitrary Lewis numbers, while the equation for  $\dot{m}_d$  used in Chapters 2 and 3 is valid only for Lewis numbers equal to 1.

To calculate the species mass evaporation rate  $\dot{m}_i$  and the values of the evaporation rate of species  $i$

These allow us to rewrite Equation (4.1), the corresponding initial condition and boundary condition (4.2) as:

$$R_d^2(t)W_t^0(t; \cdot) = D_l W^{00}(t; \cdot); \quad (4.15)$$

where  $t \geq 0$ ,

$$W(t; \cdot)|_{t=0} = W_0(\cdot) = R_{d0}^{3-2} Y_{l;0}(R_{d0}) \exp\left\{-\frac{R_d^0(0)R_{d0}}{4D_l}\right\}; \quad (4.16)$$

$$W(t; \cdot)|_{j=0} = 0; \quad (4.17)$$

$$\begin{aligned} & W^0(t; \cdot) + H_0(t)W(t; \cdot) \\ &= W_0(t) \frac{m}{D_l} (R_d(t))^{5-2} \exp\left\{-\frac{R_d^0(t)R_d(t)}{4D_l}\right\}; \end{aligned} \quad (4.18)$$

where:

$$H_0(t) = \frac{m}{D_l} R_d(t) - 1 - \frac{R_d^0(t)R_d(t)}{2D_l};$$

Condition (4.17) is an additional boundary condition, which follows from the requirement that  $Y_{li}(t; R)$  is a twice continuously differentiable function. When deriving (4.15) we took into account that  $d^2 R_d = dt^2 = 0$ .

Further simplification of Equation (4.15) and the corresponding initial and boundary conditions is possible when we apply this equation to a short time step. In this

The initial and boundary conditions for Equation (4.21) can be presented as:

$$V(x, 0) = W_0(x) = \frac{v_0(0)}{1 + h_0};$$

$$V(x, l) = 0; \quad \frac{dV}{dx}(x, l) + h_0 V(x, l) = 0;$$

As in Chapter 2, we look for the solution of Equation (4.21) in the form:

$$V(x, t) = \sum_{n=0}^{\infty} v_n(x) v_n(t); \quad (4.22)$$

where functions  $v_n(x)$  form the full set of non-trivial solutions to the equation:

$$\frac{d^2 v}{dx^2} + p v = 0; \quad 0 \leq x \leq l; \quad (4.23)$$

subject to boundary conditions:

$$v(0) = \frac{dv}{dx}(l) + h_0 v(l) = 0; \quad (4.24)$$

For  $p = 0$ , Equation (4.23) has no non-trivial solutions, satisfying the boundary conditions (4.24). For  $p = -\lambda^2 < 0$ , this equation has the solution:

$$v_0(x) = \sinh(\lambda_0 x); \quad (4.25)$$

where  $\lambda_0$  is the solution to the equation

$$\tanh \lambda_0 l = \frac{1}{h_0}; \quad (4.26)$$

The latter equation has three solutions (positive, negative and zero) remembering that  $h_0 < 1$ . We are interested in the positive solution to this equation only [19].

Note that this solution does not exist in the case of the heat conduction equation, when  $h_0$  is greater than 1 (see Chapter 2).

For  $p = -\lambda^2 > 0$ , Equation (4.23) has the solutions:

$$v_n(x) = \sin(\lambda_n x) \quad (4.27)$$

for  $n = 1, 2, \dots$ , where  $\lambda_n$  are the solutions to the equation

$$\tan \lambda_n l = \frac{1}{h_0}; \quad (4.28)$$

As in the case  $p < 0$  we disregard the solutions to this equation corresponding to zero and negative  $\lambda$ . A countable set of positive solutions to this equation (positive eigenvalues)  $\lambda_n$  are arranged in ascending order:

$$0 < \lambda_1 < \lambda_2 < \lambda_3 < \dots$$

It can be shown that functions  $v_n(x)$ ,  $n = 0$  are orthogonal for  $0 < x < 1$  (see Chapter 2).

The completeness of the set of functions  $v_n(x)$  for  $n = 0$  has been tested. Namely, we considered different functions not belonging to this set, and found that Fourier expansions of these functions on the set of  $\{v_n(x)\}_{n=0}^{\infty}$  coincide with the functions themselves. If the set of functions is not complete, then a Fourier expansion of

The general solution to the homogeneous equation:

$$R_d^2(t) \frac{d}{dt} n(t) + (1 - n(t)) D_I^2 n = 0 \quad (4.35)$$

can be presented as:

$$\ln(n(t) - n(0)) = (1 - n(0)) D_I^2 \int_0^t \frac{dt}{R_d^2(t)} \quad (4.36)$$

Assuming that  $R_d(t)$  is a linear function of  $t$  given by Equation (2.8), Solution (4.36) can be presented in a more explicit form:

$$n(t) = n(0) \exp \left[ \frac{(1 - n(0)) D_I^2}{R_{d0}^2} \frac{1}{1 + t} \right] \quad (4.37)$$

One can see that the following function:

$$n(t) = \frac{2}{1 + t} \quad (4.38)$$

is a solution of the homogeneous equation (4.35) for  $n(0) = 2/3$ .

Remembering that Solution (4.41) is applied to a very short time step, changes of  $v_0(t)$  in the integrand before the exponential term can be ignored. This allows us to simplify (4.41) to (see Appendix 6):

$$v_n(t) = [q_n + f_n v_0(0)] \exp\left(-\sum_{n=0}^{\infty} \frac{D_l \frac{2}{n} t}{R_{d0} R_d(t)}\right) + f_n v_0(t) - f_n v_0(0); \quad (4.42)$$

Note that  $v_n(t)$  in the form (4.40) satisfies Equation (4.33), while  $v_n(t)$  in the form (4.42) does not satisfy it. This is related to the fact that Equation (4.33) was derived under the assumption that Series (4.22), after being substituted into Equation (4.21), can be differentiated term by term (derivative of the series is equal to the series of derivatives). This assumption is valid when  $v_n(t)$  is taken in the form (4.40), but it is not valid when  $v_n(t)$  is taken in the form (4.42), as:

$$v_0(t) \frac{d^2}{dt^2} \sum_{n=0}^{\infty} f_n v_n \neq \sum_{n=0}^{\infty} f_n \frac{d^2 v_n}{dt^2}$$

(the series on the right hand side of this formula diverges). Note that Series (4.22) satisfies Equation (4.21) regardless of whether  $v_n(t)$  is taken in the form (4.40) or in the form (4.42).

Remembering (4.30) and (4.42), Equation (4.22) can be rewritten as:

$$V(t; r) = \sum_{n=0}^{\infty} v_n(t) v_n(r) = \frac{v_0(t) R}{1 + h_0 \frac{R}{R_d(t)}} + \frac{v_0(0) R}{1 + h_0 \frac{R}{R_d(t)}}; \quad (4.43)$$

where

$$v_n(t) = [q_n + f_n v_0(0)] \exp\left(-\sum_{n=0}^{\infty} \frac{D_l \frac{2}{n} t}{R_{d0} R_d(t)}\right); \quad (4.44)$$

The final equation for mass fraction inside the droplet can be presented as:

$$Y_{ii}(R) = \frac{1}{R} \frac{R_{d0} R^2}{4 D_l R_d(t)} \exp\left(-\sum_{n=1}^{\infty} \frac{D_l \frac{2}{n} t}{R_{d0} R_d(t)}\right) \sum_{n=1}^{\infty} v_n(t) \sin\left(n \frac{R}{R_d(t)}\right) + v_0(t) \sinh\left(\frac{R}{R_d(t)}\right) + \frac{v_0(0) R}{1 + h_0 \frac{R}{R_d(t)}}; \quad (4.45)$$

where  $v_n$  are given by Equations (4.44).

Having substituted (4.44) into (4.45) we can rearrange the latter equation for the short time step to

$$Y_{ii}(R) = \frac{m_i \exp\left(\frac{R_{d0}}{4 D_l} \frac{R_{d0} R_d(t) R^2}{R_d(t)}\right)}{m + \frac{R_{d0}}{2}} \frac{R_{d0}^{5-2}}{R_d^{5-2}(t)} + \frac{1}{R} \frac{R_{d0} R^2}{R_d(t)} \exp\left(-\sum_{n=1}^{\infty} \frac{D_l \frac{2}{n} t}{R_{d0} R_d(t)}\right) \sum_{n=1}^{\infty} [q_n + f_n v_0(0)] \exp\left(-\sum_{n=0}^{\infty} \frac{D_l \frac{2}{n} t}{R_{d0} R_d(t)}\right) \sin\left(n \frac{R}{R_d(t)}\right) + v_0(t) \sinh\left(\frac{R}{R_d(t)}\right) + \frac{v_0(0) R}{1 + h_0 \frac{R}{R_d(t)}};$$

$$[q_0 + f_{00}(0)] \exp \left[ \frac{D_l}{R_{d0} R_d(t)} \frac{z^2}{2} \right] \sinh \left[ \frac{R}{R_d(t)} \right] ; \quad (4.46)$$

When  $\alpha = 0$  but  $\beta \neq 0$  during the time step, Equation (4.46) can be further simplified to

$$Y_{li}(R) = \frac{1}{R} \sum_{n=1}^{\infty} \frac{1}{R_d(t)} \left[ q_n + f_{n0}(0) \right] \exp \left[ \frac{D_l}{R_{d0} R_d(t)} \frac{z^2}{2} \right] \sinh \left[ \frac{R}{R_d(t)} \right] + [q_0 + f_{00}(0)] \exp \left[ \frac{D_l}{R_{d0} R_d(t)} \frac{z^2}{2} \right] \sinh \left[ \frac{R}{R_d(t)} \right] ; \quad (4.47)$$

This equation is identical to Equation (13) of [38]. Note that in [38] and [50] the norm of  $v_n$  ( $\|v_n\|^2$ ) is dimensional. The ratio of  $\|v_n\|^2$  used in [38, 50] and in this Chapter is equal to  $R_{d0}$ .

Let us now relax our assumption that  $H_0(t) = h_0 = \text{const}$  and assume that:

$$H_0(t) = h_0 + h_1(t); \quad (4.48)$$

where  $h_0 = \text{const} < 1$ . In view of (4.48) we can rewrite the boundary condition at  $z = 1$  for Equation (4.15) in the form:

$$h_0 W'(z; t) + h_1 W'(z; t) \Big|_{z=1} = -\alpha_0(t) - h_1(t) W(z; 1) - \beta_0(t); \quad (4.49)$$

Assuming that  $\beta_0(t)$  is known, we can formally use the previously obtained solutions (4.20) and (4.22) to present the solution to Problem (4.15)-(4.18) in the form:

$$W(z; t) = \frac{\beta_0(t)}{1 + h_0} + V(z; t) = \sum_{n=0}^{\infty} v_n(z) q_n \exp \left[ \frac{D_l}{R_{d0} R_d(t)} \frac{z^2}{2} \right] - \sum_{n=0}^{\infty} v_n(z) \left( \frac{1}{R_{d0}} \frac{D_l}{R_d(t)} \frac{1}{R_d(t)} \right) \int_0^z \frac{\beta_0(\tau)}{R_d^2(\tau)} \exp \left[ \frac{D_l}{R_{d0} R_d(t)} \frac{\tau^2}{2} \right] d\tau ; \quad (4.50)$$

where Expression (4.41) for  $v_n(t)$  has been used.

In contrast to the previous case of  $H_0(t) = \text{const}$ , Equation (4.50) does not give us an explicit solution for  $W(z; t)$  since  $\beta_0(t)$  depends on  $W(z; 1)$ .

Equation (4.50) can be presented in a more compact form:

$$W(z; t) = V(z; t) - \int_0^z \beta_0(\tau) G(z; \tau; t) d\tau ; \quad (4.51)$$



where

$$V(t; \mathbf{x}^1) = \sum_{n=0}^{\infty} v_n(\mathbf{x}^1) q_n \exp(-\lambda t) (1 - \exp(-\lambda t))^{n-1}$$

[50]. Since the main focus of this Chapter is on the analysis of the new physical effects produced by the droplet? moving boundary, the optimisation of the algorithm is beyond its scope (cf. the analysis of accuracy and CPU efficiency of the related algorithm, not taking into account the effects of the moving boundary, described in Section 7 of [50]). Note that the speed of convergence of the algorithm turned out to be very high. Even calculations based on 100 time steps led to almost the same results as those based on 10 time steps. In the case of 100 time steps the CPU time was less than 5 sec. Calculations were performed on a 3 GHz CPU, 2 GB RAM work station.

## 4.4 Application to bi-component droplets

### 4.4.1 Effect of species diffusion

In this section, Solution (4.47) is applied to the analysis of bi-component droplet heating and evaporation in an environment close to the one described in [38]. We

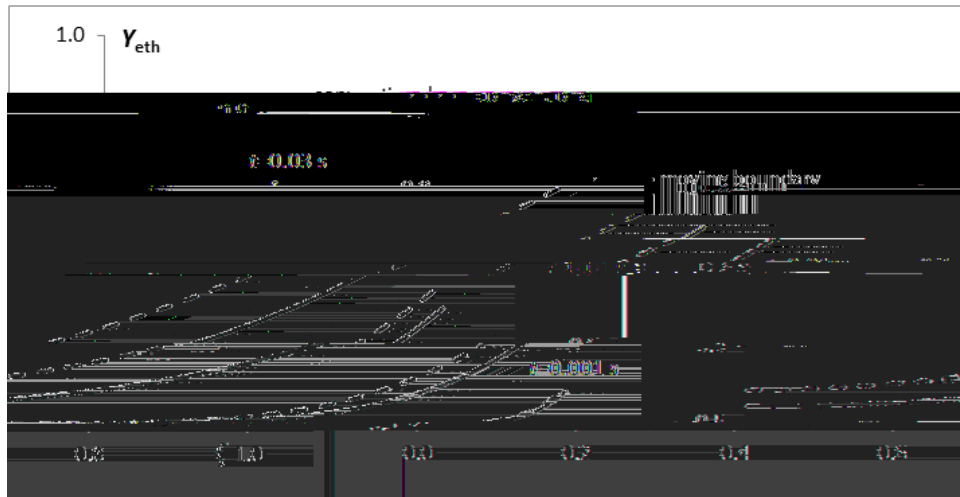


Figure 4.1: The plots of ethanol mass fraction  $Y_{\text{eth}}$  versus  $r/R_d$ , as predicted by the conventional model (dashed) and the new model, taking into account the effect of the moving boundary (solid), for times 0.001 s, 0.01 s and 0.03 s. We consider an initial 50% ethanol { 50% acetone mixture and droplets with initial diameter equal to 142.7  $\mu\text{m}$ .

shown in Fig. 4.1. As expected, both models predict the increase of  $Y_{\text{eth}}$  with increasing  $r/R_d$  and time. This is related to higher volatility of acetone in the ethanol/acetone mixture. As one can see from Fig. 4.1, at times less than 0.001 s the predictions of the conventional and the new models are practically indistinguishable. At later times, however, the new model always predicts lower values of  $Y_{\text{eth}}$  compared with the conventional model. In fact the effect of the moving boundary on the distribution of species looks stronger than a similar effect on the distribution of temperature inside droplets as reported in Chapter 2.

The plots of  $Y_{\text{eth}}$  at the droplet surface ( $Y_{\text{eth}}(r/R_d = 1)$ ) versus time, predicted by the conventional model, and the new model, taking into account the effect of the moving boundary, are shown in Fig. 4.2. As one can see from this figure, both models predict the increase of  $Y_{\text{eth}}$ (

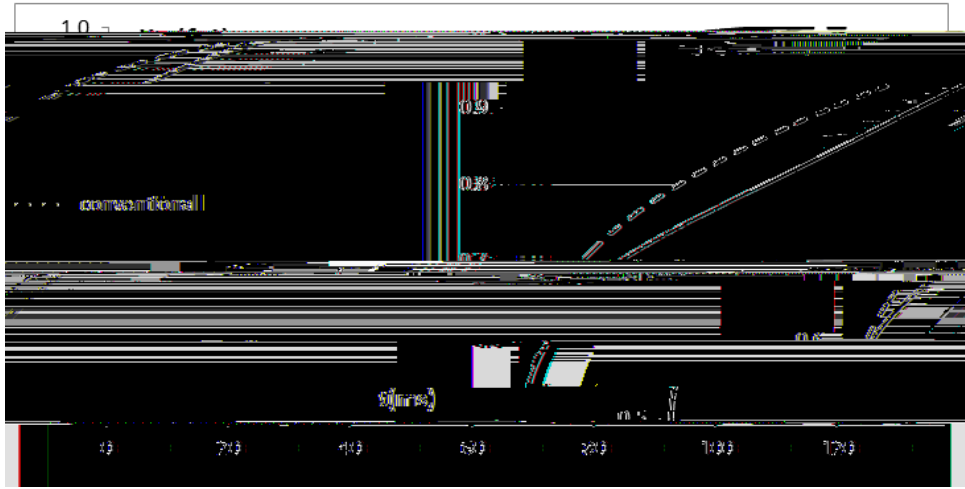


Figure 4.2: The plots of  $Y_{\text{eth}}(\ = 1)$  versus time, as predicted by the conventional model (dashed) and the new model, taking into account the effect of the moving boundary (solid).

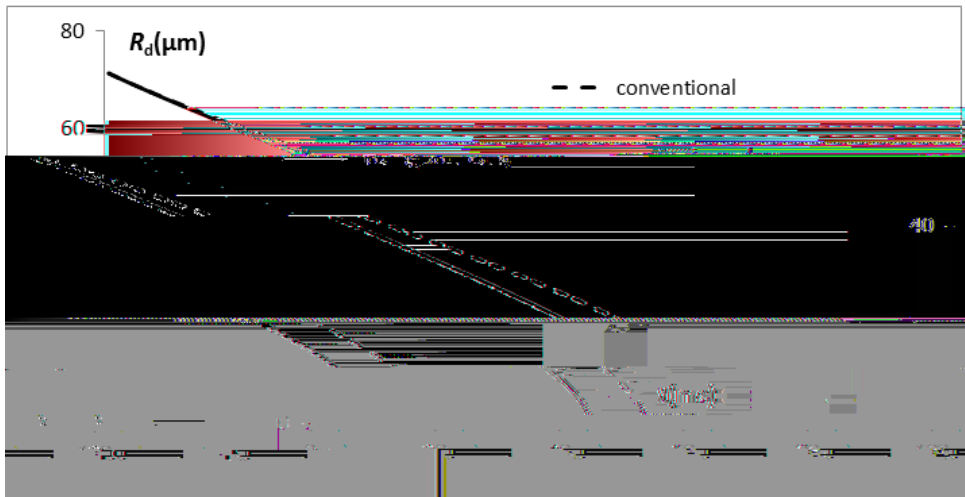


Figure 4.3: The plots of droplet radius  $R_d$  versus time, as predicted by the conventional model (dashed) and the new model, taking into account the effect of the moving boundary (solid).

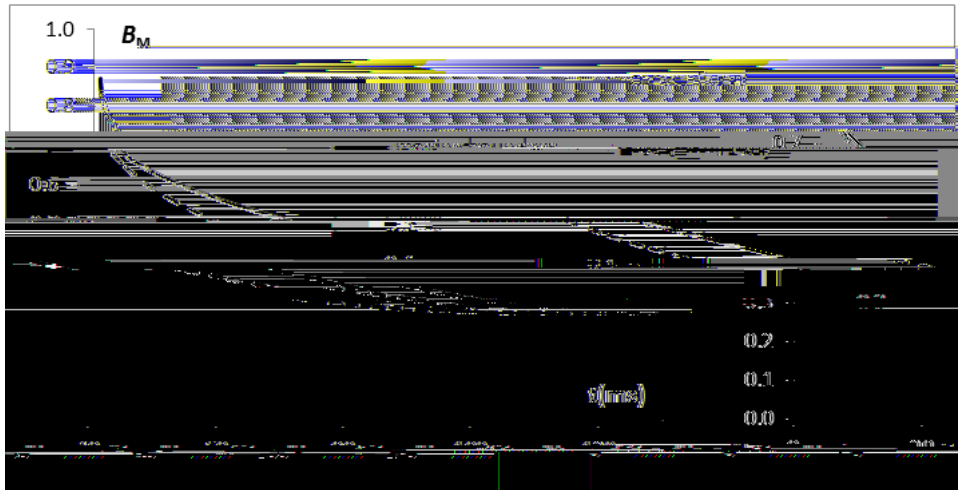


Figure 4.4: The plots of Spalding mass transfer number  $B_M$  versus time, as predicted by the conventional model (dashed) and the new model, taking into account the effect of the moving boundary (solid).

model, and the new model, taking into account the effects of the moving boundary, are shown in Fig. 4.3. As one can see from this figure, taking into account the effect of the moving boundary leads to the acceleration of droplet evaporation compared with the prediction of the conventional model. This effect is opposite to the one reported earlier for the effect of the moving boundary on the thermal conductivity inside droplets. In the latter case, the effect of the moving boundary led to slowing down of droplet evaporation. The physical background to the effect shown in Fig. 4.3 is that the new model predicts higher mass fraction of acetone at the surface of the droplet, as shown in Fig. 4.2, which evaporates faster than ethanol.

Note that for mono-component droplets at fixed temperature we would expect that the  $d^2$  law should be valid. This is obviously not the case shown in Fig. 4.3. The reason for this is that the evaporation of multi-component droplets leads to changes in the Spalding mass transfer number  $B_M$  due to the changes in vapour composition near the droplet's surface. The plots of  $B_M$  versus time, predicted by the conventional model, and the new model, taking into account the effects of the moving boundary, are shown in Fig. 4.4. As can be seen from this figure, both models predict the decrease in  $B_M$  with time except at the final stage of droplet evaporation, when the droplet becomes mono-component, consisting only of ethanol. The new model predicts larger  $B_M$  compared with the conventional model. Note that except



shown to be close to a linear function. The relevant approximations of the experimental results are summarised in Table 4.1 (reproduced from [38]).

Substance	Droplet temp.:	Diameter	Gas temp.:	Dist. parameter
100% acetone	35.1 C	143.4 m	21.5 C	7:7
100% ethanol	38.0 C	140.8 m	22.0 C	7:1
25% ethanol + 75% acetone	32.5 C	133.8 m	21.1 C	8:7
50% ethanol + 50% acetone	37.5 C	142.7 m	20.8 C	7:53
75% ethanol + 25% acetone	38.6 C	137.1 m	21.6 C	7:53

Table 4.2: The measured initial values of droplet temperature, diameter, ambient gas temperature and distance parameter for the same cases as in Table 4.1.

The measured initial values of droplet temperature, diameter, ambient gas temperature and distance parameter  $C$  (ratio of the distance between droplets to their diameters) for the same cases as in Table 4.1 are shown in Table 4.2. Gas temperature was constant during the measurements. The changes in  $C$  from the previous to the current time step were taken into account based on the following equation:

$$C_{\text{new}} = C_{\text{old}} \frac{U_{\text{drop};\text{new}}}{U_{\text{drop};\text{old}}} \frac{R_{d;\text{old}}}{R_{d;\text{new}}}; \quad (4.57)$$

where subscripts  $_{\text{new}}$  and  $_{\text{old}}$  refer to the values of variables at the previous time step and one time step behind respectively. In this case the values of  $R_{d;\text{old}}$  and  $R_{d;\text{new}}$  are known at the current time step.

The plots of time evolutions of the temperatures at the centre and the surface of the droplets and the average droplet temperatures, predicted by the models not taking into account the effect of the moving boundary and taking into account this effect for both temperature and species diffusion for the 25% ethanol { 75% acetone and 50% ethanol { 50% acetone mixture droplets, are shown in Fig. 4.5. As can be seen from this figure, the effect of the moving boundary on the predicted temperatures can be safely ignored in the analysis of experimental data described earlier. The same conclusion can be drawn for the case of the 75% ethanol { 25% acetone mixture droplets (figure is not shown).

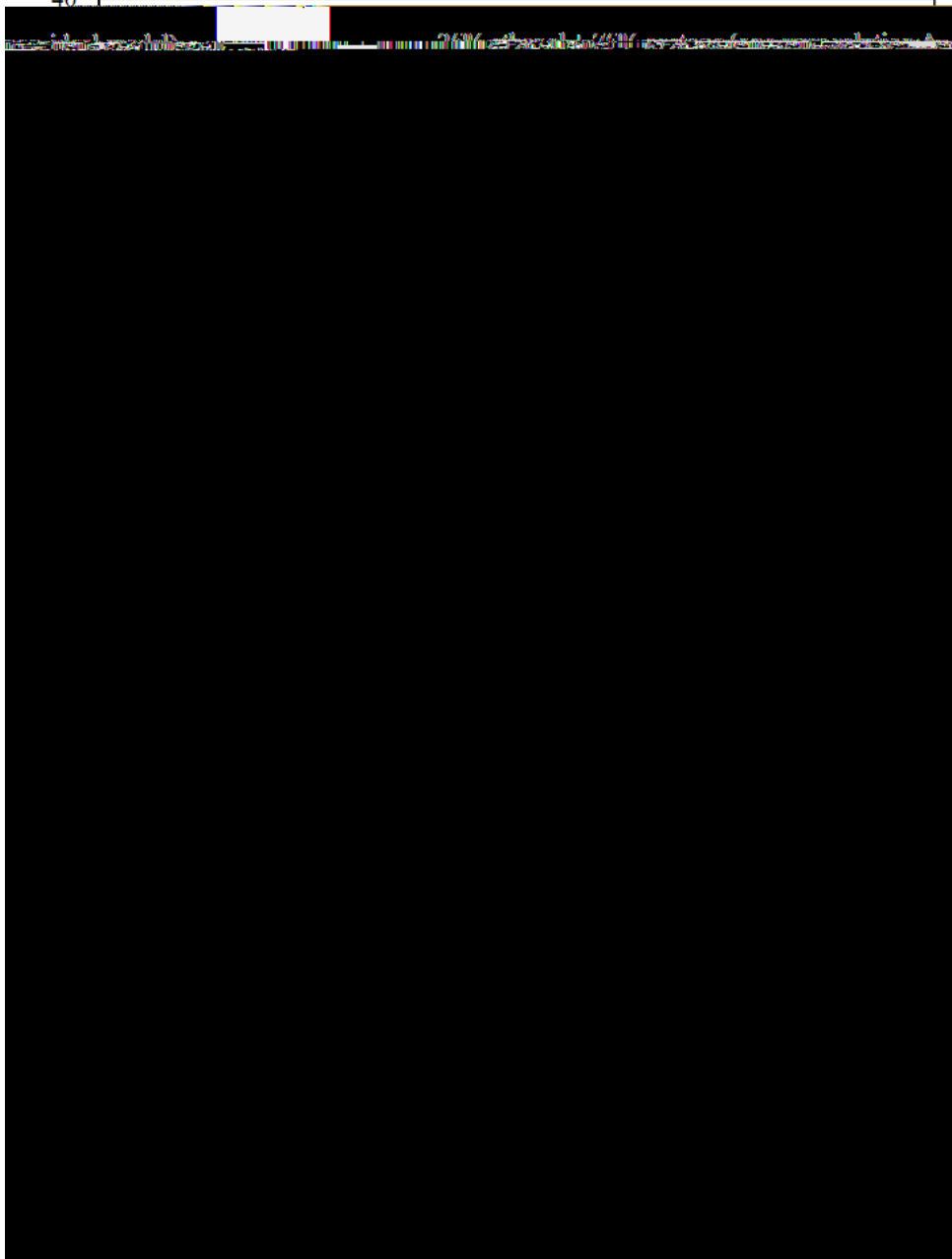


Figure 4.5: The time evolution of droplet surface, average and centre temperatures ( $T_s$ ,  $T_{av}$  and  $T_c$ ), predicted by the one-way Solution A for the non-ideal model, taking and not taking into account the effects of the moving boundary during individual time steps (moving and stationary boundaries) on the solutions to both heat transfer and species diffusion equations for the 25% ethanol { 75% acetone mixture droplets with the values of the initial parameters, droplet velocity and gas temperature given in Tables 4.1 and 4.2 (a); the same as (a) but for the 50% ethanol { 50% acetone mixture droplets (b).



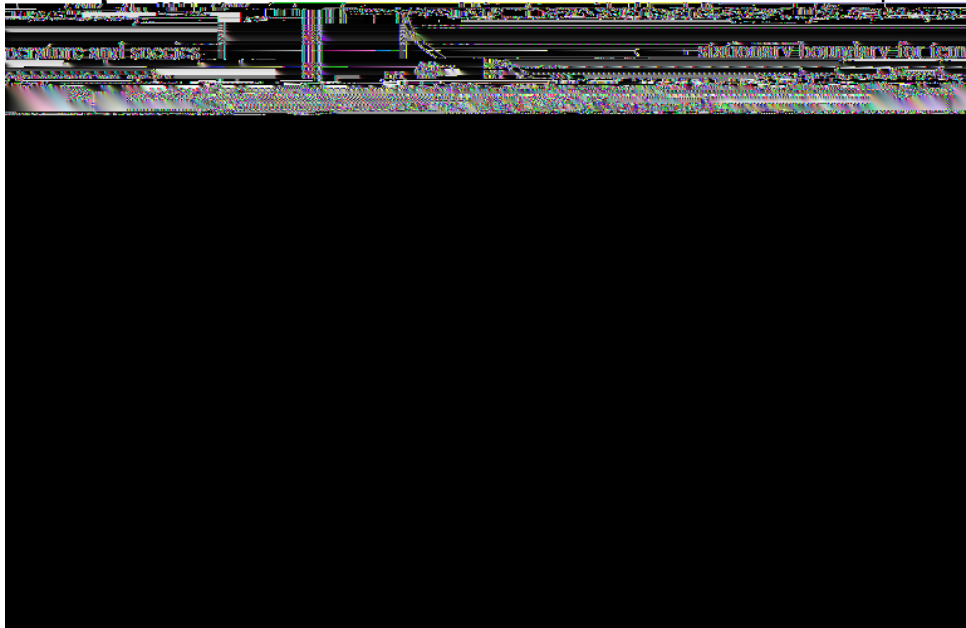


Figure 4.6: The time evolution of droplet surface temperatures ( $T_s$ ) and radius ( $R_d$ ), predicted by the one-way Solution A for the non-ideal model, taking and not taking into account the effects of the moving boundary during individual time steps on the solutions to the heat transfer equation only, species diffusion equation only and both heat transfer and species diffusion equations for the 50% ethanol { 50% acetone mixture droplets with the values of the initial parameters, and gas temperature given in Table 4.2, assuming that the droplet velocity is constant and equal to 12.71 m/s.

In Fig. 4.5 a hypothetical case is shown when the 50% ethanol { 50% acetone mixture droplets are cooled down or heated and evaporated until complete evaporation takes place. Both plots for the droplet surface temperature and droplet radius are shown. The same values as shown in Table 4.2 for the initial droplet temperature, diameter, distance parameter and gas temperature are used, but in contrast to the case shown in Table 4.1, it is assumed that the droplet velocity remains constant and equal to 12.71 m/s. The cases of the stationary boundary during individual time steps, the cases when the effects of the moving boundary are taken into account for the heat transfer and species diffusion equations separately during individual time steps, and the case when these effects are taken into account simultaneously for heat transfer and species diffusion are shown.

As can be seen from this figure, the plots taking into account the effects of

the moving boundary on the heat transfer equation only, and ignoring this effect altogether practically coincide. That means that this effect can be safely ignored for this case. Also, the plots taking into account the effects of the moving boundary on the solution to the species diffusion equation, and taking it into account for both solutions to the heat transfer and species diffusion equations practically coincide, but the difference between both these curves and the ones ignoring this effect altogether can be clearly seen after about 0.1 s. The effect of the moving boundary is a reduction of the predicted droplet surface temperature between about 0.1 to 0.6 s. During this period the droplet surface temperature is below the ambient gas temperature. Hence the reduction of the droplet surface temperature is expected to increase the heat flux from the ambient gas to the droplets, leading to the acceleration of droplet evaporation. This agrees with the predicted time evolution of the droplet radius, taking and not taking into account the effect of the moving boundary, shown in Fig. 4.6.

In Fig. 4.7 the case similar to the one shown in Fig. 4.6, but for gas temperature equal to 1000 K, is shown. In this case, droplet surface temperature increases during the whole period of droplet heating and evaporation, in contrast to the case shown in Fig. 4.6. As one can see from Fig. 4.7, the plots taking into account the effects of the moving boundary on the solution to the heat transfer equation, and ignoring this effect altogether practically coincide, as in the case shown in Fig. 4.7. Also, similarly to the case shown in Fig. 4.6, the plots taking into account the effects of the moving boundary on the solution to the species diffusion equations, and taking it into account for both heat transfer and species diffusion equations practically coincide, but the difference between both these curves and the ones ignoring this effect altogether can be clearly seen after about 5 ms. This difference between the plots is much more visible than in the case shown in Fig. 4.6. As in the case shown in Fig. 4.6, the effect of the moving boundary is to reduce the predicted droplet surface temperature leading to the increase of the heat flux from the ambient gas to the droplets and acceleration of droplet evaporation. This agrees with the predicted time evolution of droplet radius, taking and not taking into account the effect of the moving boundary, shown in Fig. 4.7.

The plots of time evolution of the surface mass fraction of ethanol  $Y_{1,s,eth}$  for the



Figure 4.7: The same as Fig. 4.6 but for the gas temperature equal to 1000 K.

same case as shown in Fig. 4.7, are shown in Fig. 4.8. Similarly to the case shown in Fig. 4.7, the main effect of the moving boundary on the solution to the species diffusion equation is its influence on the values of  $Y_{l,s,eth}$ . This effect leads to visible reductions of the values of  $Y_{l,s,eth}$  until the complete evaporation of the droplet takes place.

## 4.5 Conclusions of Chapter 4

Two new solutions to the equation, describing the diffusion of species during multi-component droplet evaporation, are suggested. The first solution is the explicit analytical solution to this equation, while the second one reduces the solution of the differential transient species diffusion equation to the solution of the Volterra integral equation of the second kind. Both solutions take into account the effect of the reduction of the droplet radius due to evaporation.

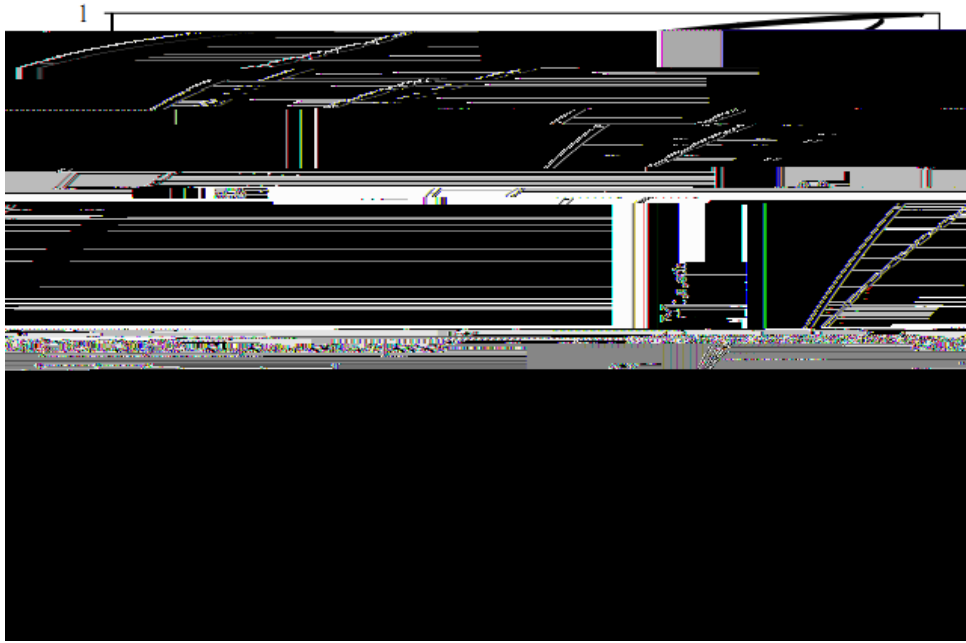


Figure 4.8: The same as Fig. 4.7 but for the mass fraction of ethanol at the surface of the droplet.

Chapter 2, which took into account the effect of the moving boundary due to droplet evaporation on the distribution of temperature inside the droplet.

The analytical solution has been incorporated into a zero dimensional CFD code and applied to the analysis of bi-component droplet heating and evaporation. The case of initial 50% ethanol { 50% acetone mixture and droplets with initial diameter equal to  $142.7 \mu\text{m}$ , as in our earlier paper [38], has been considered. Effects of droplets on gas have been ignored at this stage and droplet velocity has been assumed to be constant and equal to  $12.71 \text{ m/s}$ . To separate the effect of the moving boundary on the species diffusion equation from similar effects on the heat conduction equation inside droplets, described in previous two Chapters, a rather artificial assumption that the droplet temperature is homogeneous and fixed has been made.

It has been pointed out that the moving boundary slows down the increase in the mass fraction of ethanol (the less volatile substance in the mixture) during the evaporation process and leads to the acceleration of droplet evaporation.

It is pointed out that for the conditions of the experiment described briefly earlier,

species diffusion equations, are very close. The deviation between the predictions of these models can be ignored in this case. At the same time, the difference in the predictions of these models needs to be taken into account when the whole period of droplet evaporation up to the complete evaporation of droplets is considered. The effect of the moving boundary is shown to be much stronger for the solution to the species diffusion equation than for the solution to the heat conduction equation inside droplets.

# Chapter 5

## Transient heating of a semitransparent spherical body immersed into a gas with inhomogeneous temperature distribution

### 5.1 Introduction of Chapter 5

The main objective of this Chapter is to generalise the model described in [52] to the case when the initial gas temperature is not homogeneous in the vicinity of droplets.

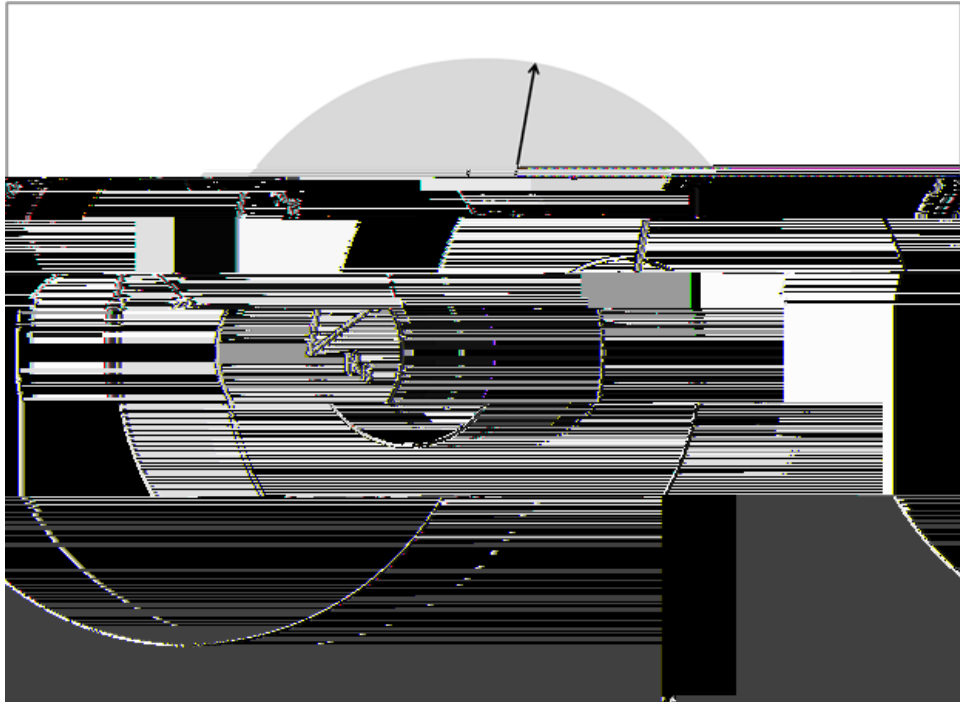


Figure 5.1: A schematic presentation of a spherical body of radius  $R_b$  immersed in the center of a gaseous sphere of radius  $R_g$ .

## 5.2 Basic equations and assumptions

As in [52], let us assume that a spherical body of radius  $R_b$  and initial temperature  $T_{b0}(R)$  is immersed in the center of a gaseous sphere of radius  $R_g$  at temperature  $T_{g0}(R)$ , as schematically shown in Fig. 5.1. The outer surface temperature of the gaseous sphere remains constant and equal to  $T_{g0}(R_g)$ .  $R_g$  is greater than  $R_b$  but finite.

The variation of the temperatures in the gas-body domain is described by the heat conduction equation in the form [105, 106]:

$$\frac{\partial T}{\partial t} = \frac{\partial^2 T}{\partial R^2} + \frac{2}{R} \frac{\partial T}{\partial R} + P(t; R); \quad (5.1)$$

where

$$\begin{cases} k = k_b = (c_b \rho_b) & \text{when } R < R_b \\ k = k_g = (c_{pg} \rho_g) & \text{when } R_b < R < R_g; \end{cases} \quad (5.2)$$

$$T(R_g) = T_{g0}(R_g) = \text{const.}$$

Equation (5.1) is identical to Equation (2.1). In contrast to Equation (2.1), however,  $k$  in Equation (5.1) is not constant and the latter Equation refers to both

liquid and gas. Equation (5.1) is the same as used in [52] except that  $T_{g0}$  is not constant but depends on  $R$  in the range  $R_b < R < R_g$ . The model for the radiation term  $P(t; R)$  is the same as used in [52].

As in [52], Equation (5.1) needs to be solved subject to initial and boundary conditions:

$$T|_{t=0} = \begin{cases} T_{b0}(R) & \text{when } R < R_b \\ T_{g0}(R) & \text{when } R_b < R < R_g \end{cases} \quad (5.3)$$

$$T|_{R=R_b} = T|_{R=R_b^+}; \quad k_b \frac{\partial T}{\partial R} \Big|_{R=R_b} = k_g \frac{\partial T}{\partial R} \Big|_{R=R_b^+}; \quad T|_{R=R_g} = T_{g0}(R_g) \quad (5.4)$$

The physical meaning of the value of  $R_g - R_b$  can be interpreted in terms of the so called 'lm' theory [44]. The key concept of this theory is thermal lm thickness  $\tau$ , the expression for which is derived from the requirement that the rate of a purely molecular transport by thermal conduction through the lm must be equal to the actual intensity of the convective heat transfer between the body surface and the external flow. For the case of heat conduction at the surface of a sphere this requirement can be written as [131]:

$$q_s^{(0)} = \frac{k_g T}{R_b \frac{R_b^2}{R_b + \tau_0}} = h T; \quad (5.5)$$

where  $q_s^{(0)} = j q_s = (4 R_b^2)$  is the value of the heat flux at the surface of the droplet,  $T = T_g - T_s$ , index 0 here indicates that the effects of the Stefan Tef 259.764.72gf 5.8533ects 92



The introduction of non-zero  $Re$  affects our earlier assumption about the spherical symmetry of the problem and  $h = k_g/R_b$ . This can be overcome if we replace  $k_g$  by

$$k_{g,e} = k_g Nu_0 = 2$$

to satisfy Equation (5.5). If the body is liquid then  $k_b$  would need to be replaced by the effective liquid thermal conductivity, following the effective thermal conductivity model [44]. These effects are not considered in this Chapter.

Note that the 'Im theory' based on Equations (5.5)-(5.8) was developed under

$$jjV_n j^2 = \frac{c_b c_b R_b}{2 \sin^2(a_b R_b)} + \frac{c_{pg} c_g (R_g - R_b)}{2 \sin^2(a_g (R_b - R_g))} \frac{k_b k_g}{2 R_b^2},$$

$$\rho_n(t) = \frac{c_b c_b}{jjV_n j^2} \int_0^{R_b} RP(t; R) v_n(R) dR:$$

A countable set of positive eigenvalues  $a_n$  is found from the solution to the equation:

$$a_n \frac{1}{k_b c_b} \cot(a_b R_b) - a_n \frac{1}{k_g c_{pg} c_g} \cot(a_g (R_b - R_g)) = \frac{k_b k_g}{R_b}. \quad (5.11)$$

These are arranged in ascending order  $0 < a_1 < a_2 < \dots$ .  $a_b = a_n \frac{c_b c_b}{k_b}$ ,  $a_g = a_n \frac{c_{pg} c_g}{k_g}$ .

Having introduced new dimensionless variables:

$$\bar{T} = \frac{T(R; t)}{T_{g0}(R_g)}; \quad \bar{T}_b = \frac{T_{b0}(R)}{T_{g0}(R_g)}; \quad \bar{T}_g = \frac{T_{g0}(R)}{T_{g0}(R_g)}; \quad r = \frac{R}{R_b}; \quad r_g = \frac{R_g}{R_b};$$

and ignoring the contribution of thermal radiation, Equation (5.9) can be simplified to

$$\bar{T} = 1 + \frac{R_b}{r} \sum_{n=1}^{\infty} \exp\left(-\frac{a_n^2 t}{jjV_n j^2}\right) \int_0^1 (1 - \bar{T}_b) r v_n(R_b r) c_b c_b dr$$

$$+ \int_0^{r_g} (1 - \bar{T}_g) r v_n(R_b r) c_{pg} c_g dr v_n(R_b r); \quad (5.12)$$

If  $T_{g0}(R) = T_{g0}(R_g) = \text{const}$  and  $T_{b0}$  does not depend on  $R$  then Equation (5.9) can be simplified to

$$T(R; t) = T_{g0} + \frac{1}{R} \sum_{n=1}^{\infty} \exp\left(-\frac{a_n^2 t}{jjV_n j^2}\right) \frac{(T_{g0} - T_{b0})^D k_b c_b c_b}{n j j V_n j^2} R_b \cot(a_b R_b) \frac{1}{n a_b}$$

$$+ \int_0^t \exp\left(-\frac{a_n^2 (t - \tau)}{jjV_n j^2}\right) \rho_n(\tau) d\tau v_n(R); \quad (5.13)$$

This solution was studied in detail in the previous paper [52].

## 5.4 Analysis

Let us consider typical values of parameters for the case when Diesel fuel droplets with an initial temperature of 300 K are injected into a gas at temperature 900 K and pressure 30 atm (situation typical for Diesel engines [42]):

$$c_b = 600 \text{ kg}\cdot\text{m}^{-3} \quad k_b = 0.145 \text{ W}\cdot\text{m}^{-1}\cdot\text{K}^{-1} \quad c_b = 2830 \text{ J}\cdot\text{kg}^{-1}\cdot\text{K}^{-1}$$

$$c_g = 23.8 \text{ kg}\cdot\text{m}^{-3} \quad k_g = 0.061 \text{ W}\cdot\text{m}^{-1}\cdot\text{K}^{-1} \quad c_{pg} = 1120 \text{ J}\cdot\text{kg}^{-1}\cdot\text{K}^{-1}:$$

This leads us to the following estimates of thermal diffusivities of the body and gas as defined by Equation (5.2):

$$k_b = 8.54 \cdot 10^{-8} \text{ m}^2\text{/s}; \quad k_g = 2.29 \cdot 10^{-6} \text{ m}^2\text{/s}:$$

Note that we took gas temperature slightly higher than the one used in [52], where it was assumed that  $T_{g0}(R_g) = 800 \text{ K}$ . The values of transport coefficients for gas were taken to be the same as in [42, 52]. The difference of the values of these coefficients for these two temperatures were ignored as in [52].

We assume that the droplets can be treated as a body the temperature of which is initially homogeneous, while  $T_{g0}(R_g) = 900 \text{ K}$  and  $R_b = 10^{-6} \text{ m}$ . Pr is assumed to be equal to 0.7 and two values of Re are considered: 1 and 5. Remembering (5.6), this leads to the following values of  $R_g$ :

$$R_{g1} = 3.301 R_b \quad \text{and} \quad R_{g2} = 11.337 R_b:$$

Two cases of the initial distribution of gas temperature in the range  $R_b < R < R_g$  are considered. Firstly, we assume that  $T_{g0}(R)$  satisfies Equation (5.8), which leads to the following expression:

$$T_{g0}(R) = T_{b0} + [T_{g0}(R_g) - T_{b0}] \frac{\frac{1}{R_b} - \frac{1}{R}}{\frac{1}{R_b} - \frac{1}{R_g}}: \quad (5.14)$$

Secondly we assume that

$$T_{g0}(R) = T_{g0}(R_g): \quad (5.15)$$

The latter case is identical to the one considered in [52].

The analysis of the effects of thermal radiation would lead to the results identical to the ones reported in [52]. This will not be considered in this work.

The analysis will be focused on the dimensionless time (Fourier number), distance and temperature defined as:

$$Fo = t_{g0} R_b^2; \quad r = R/R_b; \quad \hat{T}_{(s)} = (T_{(s)}(R; t) - T_{b0}) / (T_{g0}(R_g) - T_{b0}):$$

The calculations were performed using the package Wolfram Mathematica v 6.0 on a one 3.0 GHz Kernel. 100 terms of the series were taken.

Plots of  $\hat{T}$

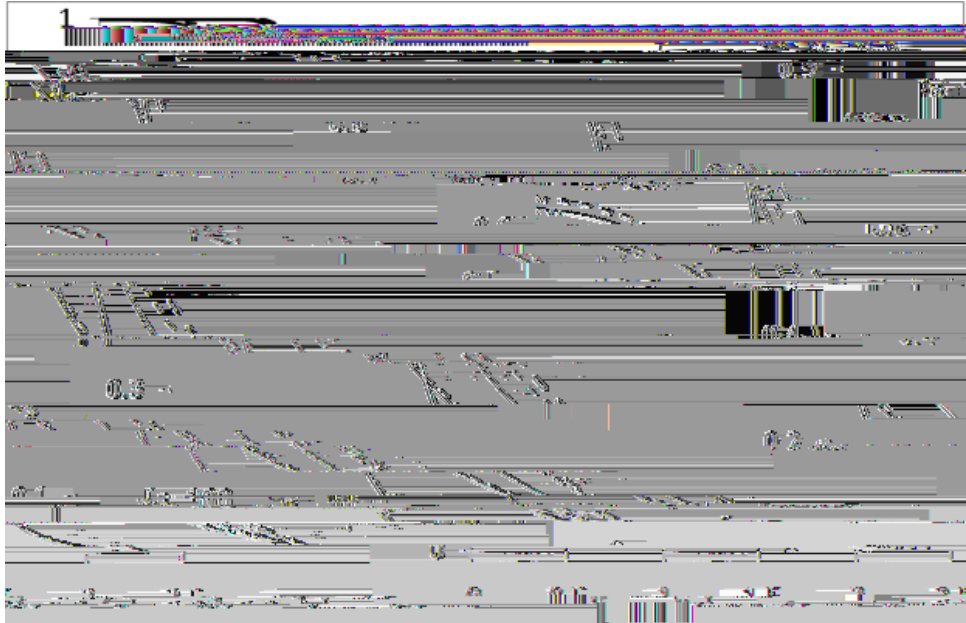


Figure 5.2: The plots of  $\hat{T} = (T_{g0}(R_g) - T(R; t)) / (T_{g0}(R_g) - T_{b0})$  versus  $r = R = R_b$  for  $r_g = R_g = R_b = 3.301$  and four Fo (indicated near the curves). Solid curves refer to the initial distribution (5.15), while dashed curves refer to the initial distribution (5.14). The thickness of the curves is inversely proportionate to Fo.

by Expressions (5.14) and (5.15). As follows from this figure, for  $Fo = 0.1$  most of the interior of the body is not affected by high gas temperature for both initial distributions of  $T_{g0}(R)$ , but the body temperatures near the surface are affected stronger by gas for distribution (5.15), compared with distribution (5.14). The difference in gas temperatures is  $\Delta T_g = 3.251 - 0 = 3.251$  K for  $T_d = [(1) - 414/F23] = 7.9701$  K for  $Tr = Fo$  (indicated)

Figure 5.3: The same as Fig. 5.2 but for  $r_g = 11.337$ .

The plots of  $\hat{T}_s$  versus Fo for  $R_g = 3.301 R_b$ ,  $R_g = 11.337 R_b$  and both initial distributions of  $T_{g0}(R)$  are shown in Fig. 5.4. As follows from this figure, the body surface is always heated quicker for distribution (5.15) compared with distribution (5.14) as expected. Also, the body is heated quicker for  $R_g = 3.301 R_b$  than for  $R_g = 11.337 R_b$ . All these results are consistent with those shown in Figs. 5.2 and

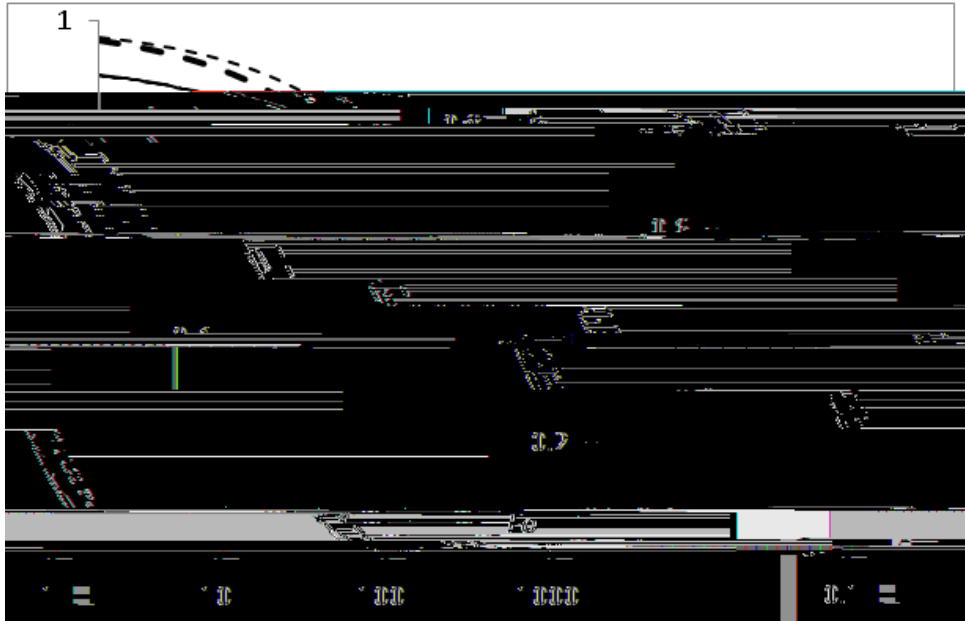


Figure 5.4: The plots of  $\hat{T}_s = (T_{g0}(R_g) - T_s(R; t)) / (T_{g0}(R_g) - T_{b0})$  versus Fo for  $r_g = 3:301$  and distribution (5.15) (solid),  $r_g = 11:337$  and distribution (5.15) (dashed-dotted),  $r_g = 3:301$  and distribution (5.14) (thick dashed),  $r_g = 11:337$  and distribution (5.14) (thin dashed).

If the Newton's law is valid then  $\hat{T}_s = 1$ . As shown in [52] for the special case of a body immersed into a homogeneous gas, this is not valid in the general transient case.

The plots of  $\hat{T}_s$  versus Fo for various  $r_g = R_g/R_b$ , and both initial distributions of  $T_{g0}(R$



Figure 5.5: The plots of

on the distance from the body surface, if this distance is less than  $R_g = R_b$ . The solution is applied to modelling body heating in conditions close to those observed in Diesel engines.

It is pointed out that inhomogeneous gas temperature distribution leads to slowing down of body heating compared with the case when the body is immersed into a homogeneous gas. In the long time limit, the distribution of temperature in the body and gas practically does not depend on the initial distribution of gas temperature.

The study of the correction of the convective heat transfer coefficient for the case of body immersion in gas with homogeneous temperature distribution confirmed the results earlier reported in [52]. For small  $Fo$ , this correction does not depend on the size of the gas domain, and reaches about 2.8 at  $Fo = 0.1$ . For  $Fo > 1$  this correction becomes sensitive to the size of the domain. For large domains it has e s o-288(it,o27aF-288e]T



# Chapter 6

## Conclusions

New solutions to the heat conduction equation, describing transient heating of an evaporating droplet, are suggested. These solutions take into account the effect of the reduction of the droplet radius due to evaporation, assuming that this radius is a linear function of time. The latter assumption does not allow us to apply these solutions to describe the whole process, from the start of evaporation, until the moment in time when the droplet completely evaporates. However, these solutions are expected to be used to describe droplet heating and evaporation over a small time step when other parameters, except droplet radius and temperature, can be assumed constant. In this case they can be considered as generalisations of the approach



the distance from the droplet centre, predict the same results. This suggests that both models are likely to be correct. It is shown that the temperatures predicted by the models based on the assumption of constant initial droplet temperature, and the one taking into account the increase in this temperature with the distance from the droplet centre, tend to converge with time.

Two new solutions to the equation, describing the diffusion of species during multi-component droplet evaporation, are suggested. Both solutions take into account the effect of the reduction of the droplet radius due to evaporation, assuming that this radius is a linear function of time. The first solution is the explicit analytical solution to this equation, while the second one reduces the solution of the differential

the species diffusion equation than for the solution to the heat conduction equation inside droplets.

The problem of heating of a body immersed into gas with inhomogeneous temperature distribution is solved analytically assuming that at a certain distance  $R_g - R_b$  from the body gas temperature remains constant. This problem is the generalisation of the problem solved earlier when gas, into which the body is immersed, is assumed to be initially homogeneous. This solution is applied to the case when the distribution of gas temperature is chosen such that heat flux in gas initially does not depend on the distance from the body surface, if this distance is less than  $R_g - R_b$ . The solution is applied to modelling body heating in conditions close to those observed in Diesel engines.

It is pointed out that inhomogeneous gas temperature distribution leads to slowing down of body heating compared with the case when the body is immersed into a homogeneous gas. In the long time limit, the distribution of temperature in the body and gas practically does not depend on the initial distribution of gas temperature. The study of the correction of the convective heat transfer coefficient for the case of body immersion in gas with homogeneous temperature distribution confirmed the results earlier reported in [52]. For small  $Fo$ , this correction does not depend on the size of the gas domain, and reaches about 2.8 at  $Fo = 0.1$ . For  $Fo > 1$  this correction becomes sensitive to the size of the domain. For large domains it has been shown to be the same as follows from the earlier model suggested in [67] for an infinitely large domain occupied by the gas. The values of this correction to Newton's law vary from about 0.1

## References

- [1] S.S. Sazhin. Advanced models of fuel droplet heating and evaporation. *Progress in Energy and Combustion Science*, 32(2):162{214, 2006.
- [2] S.S. Sazhin, I.N. Shishkova, and M.R. Heikal. Kinetic modelling of fuel droplet heating and evaporation: calculations and approximations. *International Journal of Engineering Systems Modelling and Simulation*, 2(3):169{176, 2010.
- [3] B.Y. Cao, J.F. Xie, and S.S. Sazhin. Molecular dynamics study on evaporation and condensation of n-dodecane at liquid{vapor phase equilibria. *The Journal of Chemical Physics*, 134:164309, 2011.
- [4] J.F. Xie, S.S. Sazhin, and B.Y. Cao. Molecular dynamics study of the processes in the vicinity of the n-dodecane vapour/liquid interface. *Physics of Fluids*, 23:112104, 2011.
- [5] I.N. Shishkova and S.S. Sazhin. A numerical algorithm for kinetic modelling of evaporation processes. *Journal of Computational Physics*, 218(2):635{653, 2006.
- [6] S.S. Sazhin, I.N. Shishkova, A.P. Kryukov, V.Y. Levashov, and M.R. Heikal. Evaporation of droplets into a background gas: Kinetic modelling. *International Journal of Heat and Mass Transfer*, 50:2675{2691, 2007.
- [7] S.S. Sazhin, I.N. Shishkova, T. Kristyadi, S.P. Martynov, and M.R. Heikal. Droplet heating and evaporation: hydrodynamic and kinetic models. *Heat Transfer Research*, 39(4):293{303, 2008.
- [8] S.S. Sazhin and I.N. Shishkova. A kinetic algorithm for modelling the droplet

evaporation process in the presence of heat flux and background gas. *Abi-~~atad~~ Sp*, 19:473{489, 2009.

[9]

- [19] S.S. Sazhin, P.A. Krutitskii, I.G. Gusev, and M.R. Heikal. Transient heating of an evaporating droplet. *International Journal of Heat and Mass Transfer*, 53:2826{2836, 2010.
- [20] S.S. Sazhin, P.A. Krutitskii, I.G. Gusev, and M.R. Heikal. Transient heating of an evaporating droplet with presumed time evolution of its radius. *International Journal of Heat and Mass Transfer*, 54(5-6):1278{1288, 2011.
- [21] I.G. Gusev, P.A. Krutitskii, S.S. Sazhin, and A.E. Elwardany. New solutions

- [27] S.S. Sazhin, A. Elwardany, I.G. Gusev, I.N. Shishkova, and M. Heikal. Modelling of fuel droplet heating and evaporation: recent results and unsolved problems. In *Engineering Research Advances in Amalia ad Miklosaj*, pages pp. B:197{B:209, University of Pecs, Hungary, October 25-26 2010. Pollack Mihaly Faculty of Engineering, University of Pecs.
- [28] I.G. Gusev, P.A. Krutitskii, and S.S. Sazhin. Droplet heating and evaporation in the presence of a moving boundary: numerical analysis based on analytical solutions. In *Bo d Abacs*, page 42, University of Brighton (UK), 12-14th July 2010. 11th International Conference on Integral Methods in Science and Engineering.
- [29] S.S. Sazhin, I.N. Shishkova, I.G. Gusev, A. Elwardany, P.A. Krutitskii, and M. Heikal. Fuel droplet heating and evaporation: new hydrodynamic and kinetic models. In *Bo d Abacs*, page 26, Washington, 8-13 August 2010. 11th International Conference on Integral Methods in Science and Engineering.
- [30] S.S. Sazhin, I.N. Shishkova, I.G. Gusev, and M. Heikal. Hydrodynamic and kinetic models for monocomponent droplet heating and evaporation: recent developments. In *Bo d Abacs*, page 183, Kaohsiung City, Taiwan, 2-5 November 2010. 21st International Symposium on Transport Phenomena.
- [31] S.S. Sazhin, A. Elwardany, I.G. Gusev, J.-F. Xie., B.-Y Cao, I.N. Shishkova, A.Yu. Snegirev, and M. Heikal. Modelling of complex hydrocarbon droplet heating and evaporation: hydrodynamic, kinetic and molecular dynamics approaches. In *Bo d Abacs*, Saint Petersburg, Russia, June 24-27 2011. 25th European Symposium on Applied Thermodynamics.
- [32] I.G. Gusev, S.S. Sazhin, and M. Heikal. The effects of the moving boundary on the heating of evaporating droplets. In *Proceedings ILASS Ep 2011*, page 119, Estoril, Portugal, 5-7 September 2011. 24th European Conference on Liquid Atomization and Spray Systems.
- [33] S.S. Sazhin, I.G. Gusev, M. Heikal, and P.A. Krutitskii. Modelling of liquid droplet heating and evaporation taking into account the effects of the moving boundary. In *Program ad Bo d Abacs*, page 75, Kyoto, 22{26 September



2011. The Asian Symposium on Computational Heat Transfer and Fluid Flow - 2011 (ASCH2011).

- [34] G. Miliuskas. Regularities of unsteady radiative-convective heat transfer in evaporating semitransparent liquid droplets. *International Journal of Heat and Mass Transfer*, 44:785-798, 2001.
- [35] A.D. Polyinin, A.M. Kutepov, A.V. Vyazmin, and D.A. Kazenin. *High Temperature and High Pressure in Chemical Engineering*. Taylor & Francis, 2002.
- [36] A. Faghri and Y. Zhang. *Two-Phase Flow and Heat Transfer*. Academic Press, 2006.
- [37] S. Sazhin. Modelling of sprays using computational fluid dynamics codes. *Progress in Energy and Power Engineering*, 4(1):5-16, 2009.
- [38] S.S. Sazhin, A. Elwardany, P.A. Krutitskii, G. Castanet, F. Lemoine, E.M. Sazhina, and M.R. Heikal. A simplified model for bi-component droplet heating and evaporation. *International Journal of Heat and Mass Transfer*, 53(21-22):4495-4505, 2010.
- [39]

- [43] V. Bykov, I. Goldfarb, V. Goldshtein, and J.B. Greenberg. Thermal explosion in a hot gas mixture with fuel droplets: a two reactant model. *Combustion Theory and Modelling*, 6(2):339{359, 2002.
- [44] B. Abramzon and W.A. Sirignano. Droplet vaporization model for spray combustion calculations. *International Journal of Heat and Mass Transfer*, 32(9):1605{1618, 1989.
- [45] R.J. Haywood, R. Nafziger, and M. Renksizbulut. A detailed examination of gas and liquid transient processes in convection and evaporation. *ASME Journal of Heat Transfer*, 111:495{502, 1989.
- [46] C.H. Chiang, M.S. Raju, and W.A. Sirignano. Numerical analysis of convecting, vaporizing fuel droplet with variable properties. *International Journal of Heat and Mass Transfer*, 35(5):1307{1324, 1992.
- [47] E.M. Sazhina, S.S. Sazhin, M.R. Heikal, V.I. Babushok, and R.J.R. Johns. A detailed modelling of the spray ignition process in diesel engines. *Combustion Science and Technology*, 160(1):317{344, 2000.
- [48] G. Castanet, M. Lebouche, and F. Lemoine. Heat and mass transfer of combusting monodisperse droplets in a linear stream. *International Journal of Heat and Mass Transfer*, 48:3261{3275, 2005.
- [49] C. Maqua, G. Castanet, F. Grisch, F. Lemoine, T. Kristyadi, and S.S. Sazhin. Monodisperse droplet heating and evaporation: experimental study and modelling. *International Journal of Heat and Mass Transfer*, 51(15-16):3932{3945, 2008.
- [50] S.S. Sazhin, A.E. Elwardany, P.A. Krutitskii, V. Depredurand, G. Castanet, F. Lemoine, E.M. Sazhina, and M.R. Heikal. Multi-component droplet heating and evaporation: Numerical simulation versus experimental data. *International Journal of Thermal Sciences*, 50(7):1164{1180, 2011.
- [51] C. Bertoli and M. Migliaccio. Finite conductivity model for diesel spray evaporation computations. *International Journal of Heat and Fluid Flow*, 20(5):552{561, 1999.

- [52] S.S. Sazhin, P.A. Krutitskii, S.B. Martynov, D. Mason, M.R. Heikal, and E.M. Sazhina. Transient heating of a semitransparent spherical body. *International Journal of Thermal Sciences*, 46(5):444{457, 2007.
- [53] R.B. Bird, W.E. Stewart, and E.N. Lightfoot. *Transport Phenomena*. John Wiley & Sons, Chichester, 2002.
- [54] G. Brenn. Concentration fields in evaporating droplets. *International Journal of Heat and Mass Transfer*, 48:395{402, 2005.
- [55] C. Maqua, G. Castanet, and F. Lemoine. Bi-component droplets evaporation: temperature measurements and modelling. *Fuel*, 87:2932{2942, 2008.
- [56] G.M. Faeth. Evaporation and combustion of sprays. *Progress in Energy and Combustion Science*, 9(1-2):1{76, 1983.
- [57] A.Y. Tong and W.A. Sirignano. Multicomponent transient droplet vaporization with internal circulation: integral equation formulation and approximate solution. *Numerical Heat Transfer*, 10(3):253{278, 1986.
- [58] G. Continillo and W.A. Sirignano. Unsteady, spherically-symmetric flame propagation through multicomponent fuel spray clouds. In *Modern aspects of flame propagation* (A 91-45656 19-31), volume 1, pages 173{198. New York, Springer-Verlag, 1991.
- [59] M. Klingsporn and U. Renz. Vaporization of a binary unsteady spray at high temperature and high pressure. *International Journal of Heat and Mass Transfer*, 37:265{272, 1994.
- [60] P.L.C. Lage, C.M. Hackenberg, and R.H. Rangel. Nonideal vaporization of dilating binary droplets with radiation absorption. *Combustion and Flame*, 101:36{44, 1995.
- [61] D.J. Torres, P.J. O'Rourke, and A.A. Amsden. Efficient multicomponent fuel algorithm. *Combustion and Modelling*, 7(1):67{86, 2003.
- [62] J. Tamim and W.L.H. Hallett. A continuous thermodynamics model for multicomponent droplet vaporization. *Chemical Engineering Science*, 50(18):2933{2942, 1995.

- [63] A.M. Lippert and R.D. Reitz. Modeling of Multicomponent Fuels Using Continuous Distributions With Application to Droplet Evaporation and Sprays. *SAE Technical Paper* , SP-1306:No. 972882, 1997.
- [64] G-S. Zhu, R.D. Reitz, and Aggarwal S.K. Gas-phase unsteadiness and its influence on droplet vaporization in sub- and super-critical environments. *International Journal of Heat and Mass Transfer* , 44:3081-3093, 2001.
- [65] M. Burger, R. Schmehl, K. Prommersberger, O. Schfer, R. Koch, and S. Wittig. Droplet evaporation modelling by the distillation curve model: accounting for kerosene fuel and elevated pressures. *International Journal of Heat and Mass Transfer* , 46:4403-4411, 2003.

- [73] E. Loth. Numerical approaches for motion of dispersed particles, droplets and bubbles. *Progress in Energy and Combustion Science*, 26(3):161-223, 2000.
- [74] M. Orme. Experiments on droplet collisions, bounce, coalescence and disruption. *Progress in Energy and Combustion Science*, 23(1):65-79, 1997.
- [75] H.A. Dwyer, P. Stapf, and R. Maly. Unsteady vaporization and ignition of a three-dimensional droplet array. *Combustion and Flame*, 121(1-2):181-194, 2000.
- [76] K. Harstad and J. Bellan. Evaluation of commonly used assumptions for

- [84] R.T. Imaoka and W.A. Sirignano. A generalized analysis for liquid-fuel vaporization and burning. *International Journal of Heat and Mass Transfer*, 48(21):4342{4353, 2005.
- [85] R.T. Imaoka and W.A. Sirignano. Transient vaporization and burning in dense droplet arrays. *International Journal of Heat and Mass Transfer*, 48(21):4354{4366, 2005.
- [86] S.G. Kandlikar and M.E. Steinke. Contact angles and interface behavior during rapid evaporation of liquid on a heated surface. *International Journal of Heat and Mass Transfer*, 45:3771{80, 2002.
- [87] S.C. Li. Spray stagnation flames. *Progress in Energy and Combustion Science*, 23(4):303{347, 1997.
- [88] C.H. Tsai, S.S. Hou, and T.H. Lin. Spray flames in a one-dimensional duct of varying cross-sectional area. *International Journal of Heat and Mass Transfer*, 48(11):2250{2259, 2005.
- [89] C. Crua, D.A. Kennaird, S.S. Sazhin, M.R. Heikal, and M.R. Gold. Diesel autoignition at elevated in-cylinder pressures. *International Journal of Engine Research*, 5(4):365{374, 2004.
- [90] S.S. Sazhin, E.M. Sazhina, and M.R. Heikal. Modelling of the gas to fuel droplets radiative exchange. *Fuel*, 79(14):1843{1852, 2000.
- [91] L.A. Dombrovsky, S.S. Sazhin, E.M. Sazhina, G. Feng, M.R. Heikal, M.E.A. Bardsley, and S.V. Mikhalovsky. Heating and evaporation of semi-transparent diesel fuel droplets in the presence of thermal radiation. *Fuel*, 80(11):1535{1544, 2001.
- [92] L.A. Dombrovsky, S.S. Sazhin, S.V. Mikhalovsky, R. Wood, and M.R. Heikal. Spectral properties of diesel fuel droplets. *Fuel*, 82(1):15{22, 2003.
- [93] L. Dombrovsky and S. Sazhin. Absorption of thermal radiation in a [(10 g 0 G [-489

- [94] S.S. Sazhin, W.A. Abdelgha ar, E.M. Sazhina, SV Mikhailovsky, S.T. Meikle, and C. Bai. Radiative heating of semi-transparent diesel fuel droplets. *Jal Heat Transfer* , 126:105, 2004.
- [95] L. Dombrovsky and S. Sazhin. Absorption of external thermal radiation in asymmetrically illuminated droplets. *Jal Heat Transfer* , 87(2):119{135, 2004.
- [96] B. Abramzon and S. Sazhin. Convective vaporization of a fuel droplet with thermal radiation absorption. *Fuel* , 85(1):32{46, 2006.
- [97] S.S. Sazhin, T. Kristyadi, W.A. Abdelgha ar, S. Begg, M.R. Heikal, S.V. Mikhailovsky, S.T. Meikle, and O. Al-Hanbali. Approximate analysis of thermal radiation absorption in fuel droplets. *Jal Heat Transfer* , 129:1246, 2007.
- [98] Ch Soret. Sur l'etat d'equilibre que prend au poin de vue de sa concentration une dissolution saline primitivement homogene dont deux parties sont portees a des temperatures di erentes. *Archives des Sciences Physiques et Naturelles* , 2:48{61, 1879.
- [99] S.R. de Groot and P. Mazur. *Nonequilibrium Thermodynamics* . Amsterdam: North-Holland Publishing Company, 1962.
- [100] R.M.L. Coelho and A. Silva Telles. Extended graetz problem accompanied by dufour and soret e ects. *Jal Heat and Mass Transfer* , 45(15):3101{3110, 2002.
- [101] A. Postelnicu. Influence of a magnetic eld on heat and mass transfer by natural convection from vertical surfaces in porous media considering Soret and Dufour e ects. *Jal Heat and Mass Transfer* , 47:1467{72, 2004.
- [102] V. Gopalakrishnan and J. Abraham. E ects of multicomponent diffusion on predicted ignition characteristics of an n-heptane diffusion flame. *Combustion and Flame* , 136:557{566, 2004.





- [113] S. Savovic and J. Caldwell. Finite-difference solution of one-dimensional Stefan problem with periodic boundary conditions. *International Journal of Heat and Mass Transfer*, 46:2911{2916, 2003.
- [114] S. Kutluay, A.R. Bahadir, A. Ozdes, S. Kutluay, AR Bahadir, and A. Ozdes. The numerical solution of one-phase classical stefan problem. *Journal of Computational and Applied Mathematics*, 81(1):135{144, 1997.
- [115] P.C. Meek and J. Norbury. Nonlinear moving boundary problems and a Keller box scheme. *SIAM Journal of Numerical Analysis*, 21:883{893, 1984.
- [116] S.L. Mitchell and M. Vynnycky. Finite-difference methods with increased accuracy and correct initialization for one-dimensional Stefan problems. *Applied*

- metries. *Communications in Numerical Methods in Engineering*, 16:569{583, 2000.
- [123] J. Caldwell and C.K. Chiu. Numerical solution of one-phase Stefan problems by the heat balance integral method, Part II - special small time starting procedure. *Communications in Numerical Methods in Engineering*, 16:585{593, 2000.
- [124] T.R. Goodman. The heat-balance integral and its application to problems involving a change of phase. *Transactions of the ASME Journal of Heat Transfer*, 80(2):335{342, 1958.
- [125] S.L. Mitchell and T.G. Myers. A heat balance integral method for one-dimensional finite ablation. *AIAA Journal of Thermophysics and Heat Transfer*, 22(2): 508{514, 2008.
- [126] S.L. Mitchell and T.G. Myers. Approximate solution methods for one-dimensional solidification from an incoming fluid. *Applied Mathematical Computation*, 202(1):311{326, 2008.
- [127] T.G. Myers, S.L. Mitchell, G. Muchatibaya, and M.Y. Myers. A cubic heat balance integral method for one-dimensional melting of a finite thickness layer. *International Journal of Heat and Mass Transfer*, 50: 5305{5317, 2007.
- [128] T.G. Myers. Optimizing the exponent in the heat balance and refined integral methods. Submitted to Int. Comm. Heat & Mass Trans., 2008.
- [129] S.L. Mitchell and T.G. Myers. Application of standard and refined heat balance integral methods to one-dimensional Stefan problems. *SIAM Review*, 52(1): 57{86, 2010.
- [130] A.N. Tikhonov and A.A. Samarsky. *Equations of Mathematical Physics*. Nauka Publishing House, 1972 (in Russian).
- [131] F.P. Incropera and D.P. DeWitt. *Fundamentals of Heat and Mass Transfer*. John Wiley & Sons, New York, 1996.
- [132] V. S. Vladimirov. *Equations of Mathematical Physics*. Marcel Dekker, N, 1971.

# Appendices

## Appendix 1

Convergence of the Series in  $G_1(t; \cdot)$  and Estimate of  $G_1(t; \cdot)$  at  $t \neq 0$

Let us assume that

$$0 < t < t_e = 1 =$$

and introduce the new function:

$$f(t; \cdot) = \frac{1}{R_{d0}} \frac{1}{R_d(t)} \frac{1}{R_d(\cdot)} = \frac{t}{R_d(t)R_d(\cdot)} \quad (A11)$$

In the case of a time step,  $t_e$  needs to be replaced by  $t$ . As it was done earlier, to simplify the notation it is assumed that  $t_0$  (the start of the time step) is equal to zero. This comment and assumption apply to both Appendices 1 and 2. Note that

$$f(t; \cdot) = \frac{t}{R_{d0}^2} \quad (A12)$$

since  $t < 0$  and  $R_d(t) = R_{d0}$ .

It follows from (2.31) and the estimate  $n > n$  for  $n > 1$  that  $\sum_{n=1}^{\infty} v_n j_j^2 > 1 = 4$  for  $n > 1$ . Therefore:

$$\sum_{n=1}^{\infty} v_n j_j^2 = c_0; \quad n = 1; \quad (A13)$$

where  $c_0 = \min \sum_{n=1}^{\infty} v_n j_j^2; 1 = 4$  is a positive constant.

Condition (A12) allows us to make the following estimate:

$$\exp \left( \sum_{n=1}^{\infty} f(t; \cdot) \right) = \exp \left( n^2 \frac{t}{R_{d0}^2} \right); \quad n > 1; \quad (A14)$$

where we took into account that  $n > n$  for  $n > 1$  (see Equation (17) in [15]). Using (A14) one can conclude that the series in  $G_1(t; \cdot)$  converges absolutely and

uniformly to the continuous function for  $(t; \epsilon) \in [0; 1]$  for any small  $\epsilon > 0$  since:

$$\left| \exp\left(-n^2 \frac{t}{R_{a0}^2}\right) - \exp\left(-n^2 \frac{t}{R_{a0}^2}\right) \right| \leq \epsilon \quad (A15)$$

Indeed, each term with  $n > 1$  in the series in  $G_1(t; \epsilon)$  for  $(t; \epsilon) \in [0; 1]$  can be majorized by the corresponding term of the convergent number series

$$c_0^{-1} \exp\left(-n^2 \frac{t}{R_{a0}^2}\right)$$

Now we estimate  $G_1(t; \epsilon)$  for small  $t > 0$ . Inequalities (A13) and (A14) allow us to write:

$$\begin{aligned} |G_1(t; \epsilon)| &\leq c_0^{-1} \left( 1 + \sum_{n=2}^{\infty} \exp\left(-n^2 \frac{t}{R_{a0}^2}\right) \right) \\ &\leq c_0^{-1} \left( 1 + \sum_{n=2}^{\infty} \exp\left(-n^2 \frac{t}{R_{a0}^2}\right) \right) G(t; \epsilon) \end{aligned} \quad (A16)$$

The sum  $\sum_{n=2}^{\infty} \exp\left[-n^2 \frac{t}{R_{a0}^2}\right]$  can be considered as a sum of areas of polygons of unit width placed under the curve  $\exp\left[-y^2 \frac{t}{R_{a0}^2}\right]$ . This sum is less than the area under this curve. Hence,

$$\begin{aligned} \sum_{n=2}^{\infty} \exp\left[-n^2 \frac{t}{R_{a0}^2}\right] &< \int_1^{\infty} \exp\left[-y^2 \frac{t}{R_{a0}^2}\right] dy \\ &< \int_0^{\infty} \exp\left[-y^2 \frac{t}{R_{a0}^2}\right] dy = \frac{R_{a0}}{\sqrt{t}} \int_0^{\infty} \exp\left[-z^2\right] dz \\ &= \frac{R_{a0}}{\sqrt{t}} \end{aligned} \quad (A17)$$

Having substituted (A17) into (A16) we obtain:

$$\begin{aligned} |G_1(t; \epsilon)| &\leq c_0 \left( 1 + \frac{R_{a0}}{\sqrt{t}} \right) \epsilon < \epsilon \frac{R_{a0}}{\sqrt{t}}; \\ t &\in (0; t_0]; \end{aligned} \quad (A18)$$

for any small fixed  $t_0 \in (0; 1]$ . The new constant  $\epsilon$  depends on  $t_0$ . Inequality (A18) holds uniformly for  $t \in [0; 1]$ .

## Appendix 2

### Numerical solution of Equation (2.51)

Let  $(t) = W(t;1)$  and rewrite Equation (2.51) as:

$$(t) = V(t;1) \int_0^t [o(\tau) + h_1(\tau) ( \tau )] G(t; \tau; 1) d\tau \quad (A21)$$

We look for the solution of Equation (A21) for  $t \in [0; \hat{t}]$ , where  $\hat{t}$  is a constant,  $\hat{t} < t_e$ . Let  $t = \hat{t} = N \Delta t$  and  $t_n = n \Delta t$ , where  $N$  is the total number of time steps,  $n = 0; 1; \dots; N$  is the number of the current time step. Note that  $t_0 = 0$  and  $t_N = \hat{t}$ . Discretisation of Equation (A21) gives:

$$(t_n) = V(t_n;1) \sum_{j=1}^n \int_{t_{j-1}}^{t_j} [o(\tau) + h_1(\tau) ( \tau )] G(t_n; \tau; 1) d\tau \quad (A22)$$

where  $n = 1; \dots; N$ . Note that  $(t_0) = (0) = V(0;1) = W_0(1)$  is a known constant.

The first  $(n-1)$  integrals in this sum can be approximated as:

$$\int_{t_{j-1}}^{t_j} [o(\tau) + h_1(\tau) ( \tau )] G(t_n; \tau; 1) d\tau \approx f_{o(j)} + h_1(j) [ (t_j) + (t_{j-1}) ] = 2g G(t_n; j; 1) \Delta t \quad (A23)$$

where  $j = 1; 2; \dots; n-1$ ,  $j = t_j - \frac{1}{2} \Delta t$ . Approximation (A23) is valid since all functions in the integrand are continuous and we look for the solution in the class of continuous functions.

In Approximation (A23) the known functions are taken at  $\tau = j$  (middle of the range  $[t_{j-1}; t_j]$ ), while the unknown functions are taken as the average of the values at the end points  $t_{j-1}$  and  $t_j$ .

The last term in the sum in Equation (A22) requires special investigation since the kernel  $G(t_n; \tau; 1)$  in the integrand becomes singular when  $\tau \rightarrow t_n = 0$  (see Estimate (A18)). All other functions in this integrand, including the unknown function  $(t)$ , are assumed continuous. Hence, we can write:

$$\int_{t_{n-1}}^{t_n} [o(\tau) + h_1(\tau) ( \tau )] G(t_n; \tau; 1) d\tau \approx \left( o(t_n) + h_1(t_n) \frac{(t_n) + (t_{n-1})}{2} \right) \int_{t_{n-1}}^{t_n} G(t_n; \tau; 1) d\tau \quad (A24)$$

In view of Series (2.53) we can write:

$$\int_{t_{n-1}}^{t_n} G(t_n; \tau; 1) d\tau$$

$$\begin{aligned}
&= 2 \sum_{m=1}^{\infty} \frac{X^m}{h_0^2 + h_0 + \frac{2}{m}} \frac{Z_{t_n}}{R_d(t_{n-1})} \frac{1}{R_d(t_n)} \exp \left[ -\frac{2}{m} \frac{1}{R_d(t_n)} \frac{1}{R_d(t_{n-1})} \right] \\
&= 2 \sum_{m=1}^{\infty} \frac{X^m}{h_0^2 + h_0 + \frac{2}{m}} \frac{1}{R_d(t_n)} \exp \left[ -\frac{2}{m} \frac{1}{R_d(t_n)} \frac{1}{R_d(t_{n-1})} \right] \\
&= 2 \sum_{m=1}^{\infty} \frac{X^m}{h_0^2 + h_0 + \frac{2}{m}} \frac{1}{R_d(t_n)} \exp \left[ -\frac{2}{m} \frac{1}{R_d(t_n)} \frac{1}{R_d(t_{n-1})} \right] \\
&= 2 \sum_{m=1}^{\infty} \frac{X^m}{h_0^2 + h_0 + \frac{2}{m}} \frac{1}{R_d(t_n) R_d(t_{n-1})} \exp \left[ -\frac{2}{m} \frac{t}{R_d(t_n) R_d(t_{n-1})} \right] \\
&= \frac{1}{1 + h_0} + 2 \sum_{m=1}^{\infty} \frac{X^m}{h_0^2 + h_0 + \frac{2}{m}} \exp \left[ -\frac{2}{m} \frac{t}{R_d(t_n) R_d(t_{n-1})} \right] g_n \quad (A25)
\end{aligned}$$

If  $h_0 = 0$  then  $m = (m - 1) =$

Using the same discretisation by  $t$  and  $\tau$  as above, we can present the discretised form of this representation as:

$$\begin{aligned}
 W(\hat{t}; \tau) &= V(\hat{t}; \tau) \sum_{j=1}^N \int_{t_{j-1}}^{t_j} \hat{\rho}_0(\tau) G(\hat{t}; \tau; \tau) d\tau \\
 &= V(\hat{t}; \tau) \sum_{j=1}^{N-1} \frac{\hat{\rho}_0(t_{j-1}) + \hat{\rho}_0(t_j)}{2} G(\hat{t}; \tau; \tau) \tau + \frac{\hat{\rho}_0(t_{N-1}) + \hat{\rho}_0(t_N)}{2} \\
 &\quad \int_{t_{N-1}}^{t_N} G(t_N; \tau; \tau) d\tau : \tag{A29}
 \end{aligned}$$

Note that  $t_N = \hat{t}$ . If  $N = 1$  then the sum in Equation (A29) is equal to zero. The last integral in Equation (A29) is improper and needs to be calculated separately. Remembering the definition of  $G(t; \tau; \tau)$ , and almost repeating the derivation of Equation (A25), we can write:

$$\begin{aligned}
 \int_{t_{N-1}}^{t_N} G(t_N; \tau; \tau) d\tau &= 2 \sum_{m=1}^M \frac{h_0^2 + \frac{\tau^2}{m}}{h_0^2 + h_0 + \frac{\tau^2}{m}} \frac{\sin \frac{\tau}{m} \sin \frac{\tau}{m}}{\frac{\tau}{m}} \\
 &\quad \left( 1 - \exp \left[ -\frac{\tau}{R_d(t_N) R_d(t_{N-1})} \right] \right) \\
 &= \frac{1}{1 + h_0} + 2 \sum_{m=1}^M \frac{h_0^2 + \frac{\tau^2}{m}}{h_0^2 + h_0 + \frac{\tau^2}{m}} \frac{\sin \frac{\tau}{m} \sin \frac{\tau}{m}}{\frac{\tau}{m}} \exp \left[ -\frac{\tau}{R_d(t_N) R_d(t_{N-1})} \right] .
 \end{aligned}$$

Having substituted the latter equation into (A29), and remembering the definition of  $\hat{\rho}_0(t_j)$ , we obtain the required value of  $W(\hat{t}; \tau)$ .

## Appendix 3

### Numerical solution of the integral Equation (3.10)

Remembering Equations (3.6) and (3.8) we can rewrite Equation (3.10) as:

$$\rho(t) + \int_0^t \rho(\tau) \left[ \frac{1}{t} - \frac{1}{\tau} \right] \rho(\tau) d\tau = 2 \rho_0(t); \tag{A31}$$

where:

$$\rho(\tau) = \frac{1}{2} \left[ \frac{1}{\tau} \frac{R_d(t)}{R_d(\tau)} + \rho - H(\tau) \right] \exp \left[ -\frac{1}{R_d(t)} \right]$$

$$\exp \left( \frac{(R_d(t) + (R_d(0)))^2}{4(t)} \right); \quad (A33)$$

Functions  $(t; )$  and  $!(t; )$  are continuous for  $t \in [0; t]$ . Hence, the singularity  $1 = \frac{\rho}{t}$  of the kernel in Equation (A31) is presented in an explicit form.

We look for the solution of Equation (A31) for  $t \in [0; \hat{t}]$ , where  $\hat{t} = t_e$  is an arbitrary, but fixed positive constant. Let  $t = \hat{t}N$  and  $t_n = n \hat{t}$ , where  $N$  is the total number of time steps,  $n = 0; 1; \dots; N$  is the number of the current time step. Note that  $t_0 = 0$  and  $t_N = \hat{t}$ . Discretisation of Equation (A31) gives:

$$(t_n) + \sum_{j=1}^{n-1} \frac{\rho}{t_j - t_{j-1}} \left( \frac{(t_{n; j})}{\rho \frac{t_n}{t_n}} + !(t_{n; j}) \right) d = 2 \rho_0(t_n); \quad (A34)$$

where  $n = 0; 1; \dots; N$ . Note that

$$(t_0) = (0) = 2 \rho_0(0)$$

is the known constant derived in Appendix 5.

The first  $(n-1)$  terms in the sum in Equation (A34) can be approximated as:

$$\sum_{j=1}^{n-1} \frac{\rho}{t_j - t_{j-1}} \left( \frac{(t_{n; j})}{\rho \frac{t_n}{t_n}} + !(t_{n; j}) \right) d \approx \frac{(t_j) + (t_{j-1})}{2} \left( \frac{(t_{n; j})}{\rho \frac{t_n}{t_n}} + !(t_{n; j}) \right) t; \quad (A35)$$

where  $j = 1; 2; \dots; n-1$ ;  $j = t_j - \frac{t}{2}$ . This approximation is valid since all functions in the integrand are continuous, and we look for the solution in the class of continuous functions  $(t)$  should be continuous for  $t \in [0; t]$ . In this approximation the known functions are taken at the points  $t = t_j$  (middle of the time interval  $[t_{j-1}; t_j]$ ), while the unknown function is taken as an arithmetic mean of its values at the times  $t_{j-1}$  and  $t_j$ .

The last term in the sum in Equation (A34) has an integrable singularity  $1 = \frac{\rho}{t}$  when  $t \rightarrow 0$  (recall that functions  $(t; )$  and  $!(t; )$  are continuous for  $t \in [0; t]$ ).

This allows us to approximate this term as:

$$\begin{aligned} & \sum_{t_n-1}^{t_n} \left( \frac{(t_{n; n})}{\rho \frac{t_n}{t_n}} + !(t_{n; n}) \right) d \\ & \approx \frac{(t_n) + (t_{n-1})}{2} \int_{t_{n-1}}^{t_n} \left( \frac{(t_{n; n})}{\rho \frac{t_n}{t_n}} + !(t_{n; n}) \right) \frac{d}{t} \\ & = (t_n) \left( \frac{\rho}{t_n} \right) \end{aligned}$$



where

$$g_n = (t_n; n)^{\rho} \frac{t}{t+1} + \frac{!(t_n; n) t}{2}$$

latter equation which will enable us to simplify the notation. Let us rewrite this equation as:

$$v(R; \hat{t}) = \sum_{j=1}^{N-1} \int_{t_{j-1}}^{t_j} G(\hat{t}; R) dt; \quad (A41)$$

where  $\hat{t} = t_N$ ,  $t_n = n \Delta t$ ,  $n = 0; 1; 2; \dots; N$ ,  $\Delta t = \hat{t}/N$ . In all integrals we can replace  $G(\hat{t}; R)$  with the average values over the corresponding time interval  $(t_{j-1} + t_j)/2$ . Moreover, in all integrals, except the last one, we can replace  $G(\hat{t}; R)$  with  $G(\hat{t}_j; R)$ , where  $\hat{t}_j = (t_{j-1} + t_j)/2$ . As a result, Equation (A41) can be presented in a more explicit form:

$$v(R; \hat{t}) = \sum_{j=1}^{N-1} \frac{(t_{j-1}) + (t_j)}{2} G(\hat{t}_j; R) \Delta t + \frac{(t_{N-1}) + (t_N)}{2} \int_{t_{N-1}}^{t_N} G(\hat{t}; R) dt; \quad (A42)$$

Firstly we assume that a priori chosen  $R$  is not equal to  $R_d(\hat{t})$ . In this case  $G(\hat{t}; R)$ , as defined by Equation (3.6), approaches 0, when  $\hat{t} \rightarrow 0$ . Hence the singularity in the integrand is not present and the last time step can be treated as

## Appendix 5

### Derivation of the expression for $u_0(0)$

Having substituted Equation (3.20) into Equation (3.19) and integrating by parts we obtain:

$$U_R^0(t; R)_{R=R_d(t)} = \int_0^{Z_{Re}} (T_{d0}(\cdot)) \frac{\partial G_1(t; R; \cdot)}{\partial R} dR$$
$$= (T_{d0}(\cdot))$$

$$f_{n,0}(0) = (1)^{n,0} D_{l,n}^2 \int_0^t \frac{1}{R_d(\tau)^2} \exp\left(-\frac{D_{l,n}^2 \tau}{R_{d0}^2}\right) \frac{1}{R_d(\tau)} \frac{1}{R_d(\tau)} d\tau \quad (A61)$$

$f_{n,0}(\tau)$  in the integrand of (4.41) is taken at the beginning of the time step.

Remembering that

$$d(R_d(\tau)^{-1}) = \frac{R_{d0}^0}{R_d^2(\tau)} d\tau$$

we can rearrange the last term in (A61) to

$$\begin{aligned} & (1)^{n,0} D_{l,n}^2 \int_0^t \frac{1}{R_d(\tau)^2} \exp\left(-\frac{D_{l,n}^2 \tau}{R_{d0}^2}\right) \frac{1}{R_d(\tau)} \frac{1}{R_d(\tau)} d\tau = \\ & \frac{(1)^{n,0} D_{l,n}^2}{R_{d0}^0} \exp\left(-\frac{D_{l,n}^2 t}{R_{d0}^2}\right) \frac{1}{R_d(t)} \frac{1}{R_d(t)} \int_0^t \frac{R_{d0}^0}{R_d(\tau)^2} \exp\left(-\frac{D_{l,n}^2 \tau}{R_{d0}^2}\right) \frac{1}{R_d(\tau)} d\tau = \\ & \frac{(1)^{n,0} D_{l,n}^2}{R_{d0}^0} \exp\left(-\frac{D_{l,n}^2 t}{R_{d0}^2}\right) \frac{1}{R_d(t)} \frac{R_{d0}}{(1)^{n,0} D_{l,n}^2} \exp\left(-\frac{D_{l,n}^2 t}{R_{d0}^2}\right) \frac{1}{R_d(t)} \\ & \exp\left(-\frac{D_{l,n}^2 t}{R_{d0}^2}\right) \frac{1}{R_{d0}} \frac{1}{R_d(0)} \\ & = \frac{1}{R_{d0}} \exp\left(-\frac{D_{l,n}^2 t}{R_{d0}^2}\right) \frac{1}{R_d(t)} \frac{1}{R_d(0)} = \frac{1}{R_{d0} R_d(t)} \exp\left(-\frac{D_{l,n}^2 t}{R_{d0}^2}\right) \quad (A62) \end{aligned}$$

When deriving (A62) we took into account (2.8).

Having substituted (A62) into (A61), we obtain (4.42).

## Appendix 7

### Derivation of Formula (5.9)

Introducing a new variable

$$u = (T - T_{g0}(R_g)) R$$

we can simplify Equation (5.1) and initial and boundary conditions (5.3) { (5.4) to:

$$\frac{\partial u}{\partial t} = \frac{\partial u}{\partial R} + RP(t; R); \quad (A71)$$

$$u|_{t=0} = T_0 R \quad (A72)$$

$$u|_{R=R_b} = u|_{R=R_b^+}; \quad k_b^h R_b u_R^0 \quad u|_{R=R_b} = k_g^h R_b u_R^0 \quad u|_{R=R_b^+}; \quad u|_{R=R_g} = 0; \quad (A73)$$

where

$$T_0 = T_0(R) = \begin{cases} T_{g0}(R_g) & \text{when } R > R_b \\ T_{b0}(R) & \text{when } R_b < R < R_g \\ T_{g0}(R_g) & \text{when } R_b < R < R_g \end{cases}$$

Conditions (A73) need to be amended by the boundary condition at  $R = 0$ . Since  $T = T_{g0}$  is finite at  $R = 0$  then  $u|_{R=0} = 0$ :

We look for the solution of Equation (A71) in the form:

$$u = \sum_{n=1}^{\infty} X^n(t) v_n(R); \quad (A74)$$

where functions  $v_n(R)$  form the full set of non-trivial solutions of the eigenvalue problem:

$$\frac{d^2 v}{dR^2} + a^2 v = 0 \quad (A75)$$

subject to boundary conditions:

$$\begin{aligned} v|_{R=0} = v|_{R=R_g} = 0 \\ v|_{R=R_b} = v|_{R=R_b^+} \\ k_b R_b v|_{R=R_b} = k_g R_b v|_{R=R_b^+} \end{aligned}; \quad (A76)$$

where

$$a = \frac{1}{\rho} = \begin{cases} \frac{c_{b,b}}{k_b} & \text{when } R > R_b \\ \frac{c_{g,g}}{k_g} & \text{when } R_b < R < R_g \end{cases} \quad (A77)$$

Note that  $\rho$  has dimension  $1 = \text{time}$ . We look for the solution of Equation (A75) in the form:

$$v(R) = \begin{cases} A \sin(a_b R) & \text{when } R > R_b \\ B \sin(a_g (R - R_g)) & \text{when } R_b < R < R_g \end{cases} \quad (A78)$$

Function (A78) satisfies boundary conditions (A76) at  $R = 0$ . Having substituted function (A78) into boundary conditions (A76) at  $R = R_b$  we obtain:

$$A \sin(a_b R_b) = B \sin(a_g (R_b - R_g)); \quad (A79)$$

$$A k_b [R_b a_b \cos(a_b R_b) - a_b] = B a_g \cos(a_g (R_b - R_g))$$



$$= \frac{c_b \ b R_b}{2 \sin^2( \ n a_b R_b)} + \frac{c_{pg} \ g (R_g \ R_b)}{2 \sin^2( \ n a_g (R_b \ R_g))} \frac{k_b \ k_g}{2 R_b \ \frac{2}{n}}. \quad (A715)$$

and the expression for  $v_n(0)$  can be further simplified to:

$$v_n(0) = \frac{c_b b T_0}{j j v_n j^2 \sin(n a_b R_b)} \int_0^{R_b} R \sin(n a_b R) dR = \frac{T_0 \rho k_b c_b b}{n j j v_n j^2} R_b \cot(n a_b R_b) - \frac{1}{n a_b} : \quad (A720)$$

The solution of Equation (A718) subject to the initial condition (A720) can be written as:

$$v_n(t) = \exp\left(-\frac{2}{n} t\right) v_n(0) + \int_0^t \exp\left(-\frac{2}{n}(t-\tau)\right) p_n(\tau) d\tau : \quad (A721)$$

Equation (5.9) follows from the definition of  $u$  and Equations (A74) and (A721).

## Appendix 8

### Proof of orthogonality of $v_n(R)$ with the weight $b$

Remembering Expressions (A714) for  $v_n(R)$  we can write for  $n \neq m$ :

$$\begin{aligned} I_{nm} &= \int_0^{R_g} v_n(R) v_m(R) b dR = \frac{k_b a_b^2}{\sin(n a_b R_b) \sin(m a_b R_b)} \int_0^{R_b} \sin(n a_b R) \sin(m a_b R) dR \\ &+ \frac{k_g a_g^2}{\sin(n a_g (R_b - R_g)) \sin(m a_g (R_b - R_g))} \int_{R_b}^{R_g} \sin(n a_g (R - R_g)) \sin(m a_g (R - R_g)) dR \\ &= \frac{k_b a_b^2}{2 \sin(n a_b R_b) \sin(m a_b R_b)} \frac{\sin((n-m) a_b R_b)}{(n-m) a_b} - \frac{\sin((n+m) a_b R_b)}{(n+m) a_b} \\ &\quad + \frac{k_g a_g^2}{2 \sin(n a_g (R_b - R_g)) \sin(m a_g (R_b - R_g))} \frac{\sin((n-m) a_g (R_b - R_g))}{(n-m) a_g} - \frac{\sin((n+m) a_g (R_b - R_g))}{(n+m) a_g} \\ &= \frac{1}{2(n-m)} \frac{k_b a_b \sin((n-m) a_b R_b)}{\sin(n a_b R_b) \sin(m a_b R_b)} - \frac{k_g a_g \sin((n-m) a_g (R_b - R_g))}{\sin(n a_g (R_b - R_g)) \sin(m a_g (R_b - R_g))} \\ &+ \frac{1}{2(n+m)} \frac{k_b a_b \sin((n+m) a_b R_b)}{\sin(n a_b R_b) \sin(m a_b R_b)} + \frac{k_g a_g \sin((n+m) a_g (R_b - R_g))}{\sin(n a_g (R_b - R_g)) \sin(m a_g (R_b - R_g))} \\ &= \frac{[k_b a_b (\cot(m a_b R_b) - \cot(n a_b R_b)) - k_g a_g (\cot(m a_b (R_b - R_g)) - \cot(n a_b (R_b - R_g)))]}{2(n-m)} \\ &+ \frac{[k_b a_b (\cot(m a_b R_b) + \cot(n a_b R_b)) + k_g a_g (\cot(m a_b (R_b - R_g)) + \cot(n a_b (R_b - R_g)))]}{2(n+m)} \end{aligned}$$

Remembering Equation (A713) we can write:

$$\begin{aligned} I_{nm} &= \frac{1}{2(n-m)} \frac{k_b}{R_b} \frac{k_g}{m} - \frac{k_b}{R_b} \frac{k_g}{n} - \frac{1}{2(n+m)} \frac{k_b}{R_b} \frac{k_g}{m} + \frac{k_b}{R_b} \frac{k_g}{n} \\ &= \frac{k_b}{2R_b} \frac{k_g}{n-m} - \frac{k_b}{2R_b} \frac{k_g}{n-m} = 0: \end{aligned}$$